



Targeted Training Activity (TTA) 2017- Monsoons in a Changing Climate



SST Gradient in the Tropical Indo-Pacific Domain and The Asian Summer Monsoon Onset

**Guoxiong WU,
Jiangyu Mao, Yimin Liu, Boqi Liu , Roncai Ren**

LASG, Institute of Atmospheric Physics, CAS



Trieste, Italy, 31 Jul- 4 Aug

Outline



1

Variability of the ASM

2

Dynamics of ASM onset

亚洲夏季风爆发动力学

3

Evolution of the ASM onset

亚洲夏季风爆发过程

4

ENSO and ASM Onset

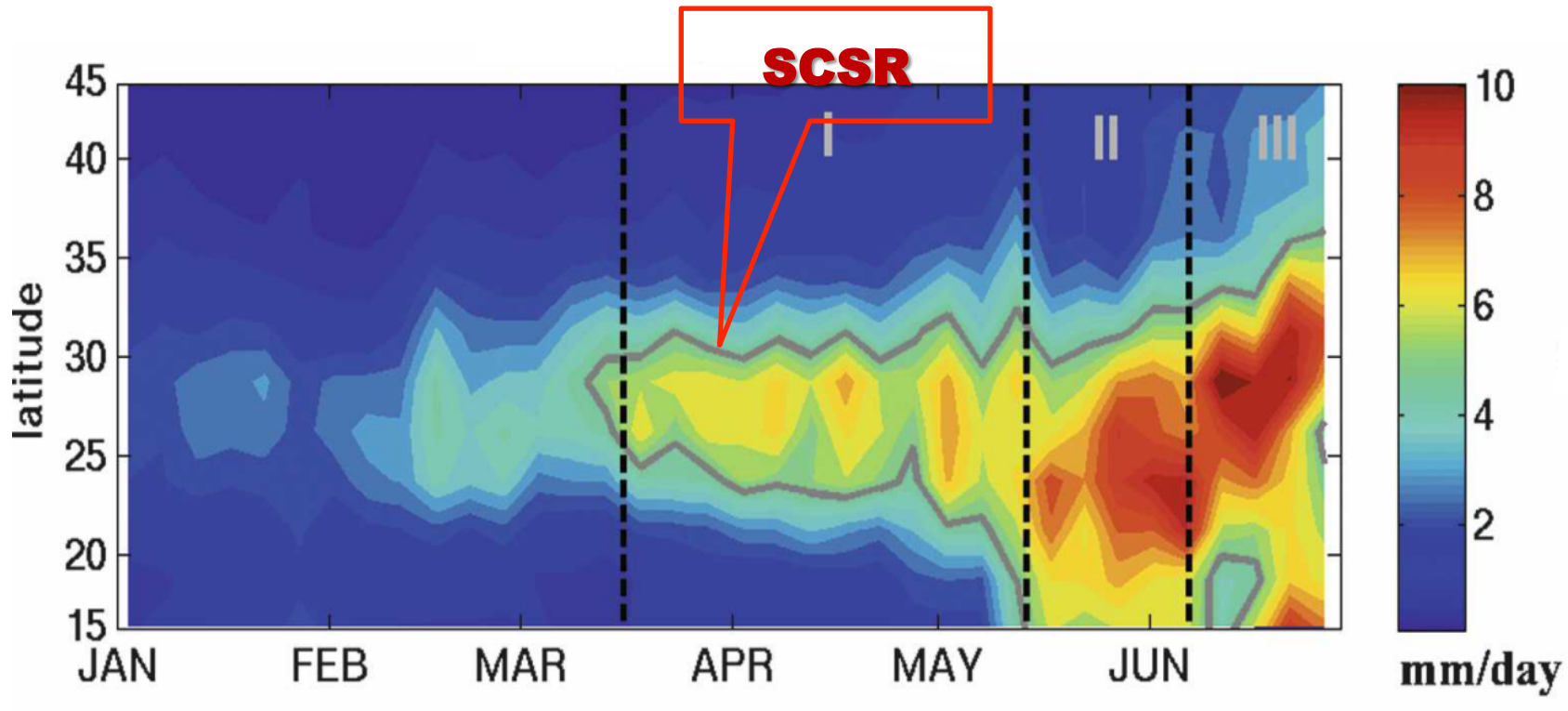
ENSO和亚洲夏季风爆发

5

Summary 结论



110°-130°E averaged precipitation



LinHo等(2008)

降水年际变率大，致使旱涝灾害频繁

春季连阴雨天气是华南地区常见的一种灾害性天气

季节内振荡是全球大气多时间尺度振荡现象的重要组成部分，是联系天气与气候的直接纽带，对阶段性、持续性极端事件的发生具有重要影响

□ 理解季节内振荡如何影响华南春季气候

□ 提高华南春季延伸期以及月季降水趋势预测能力

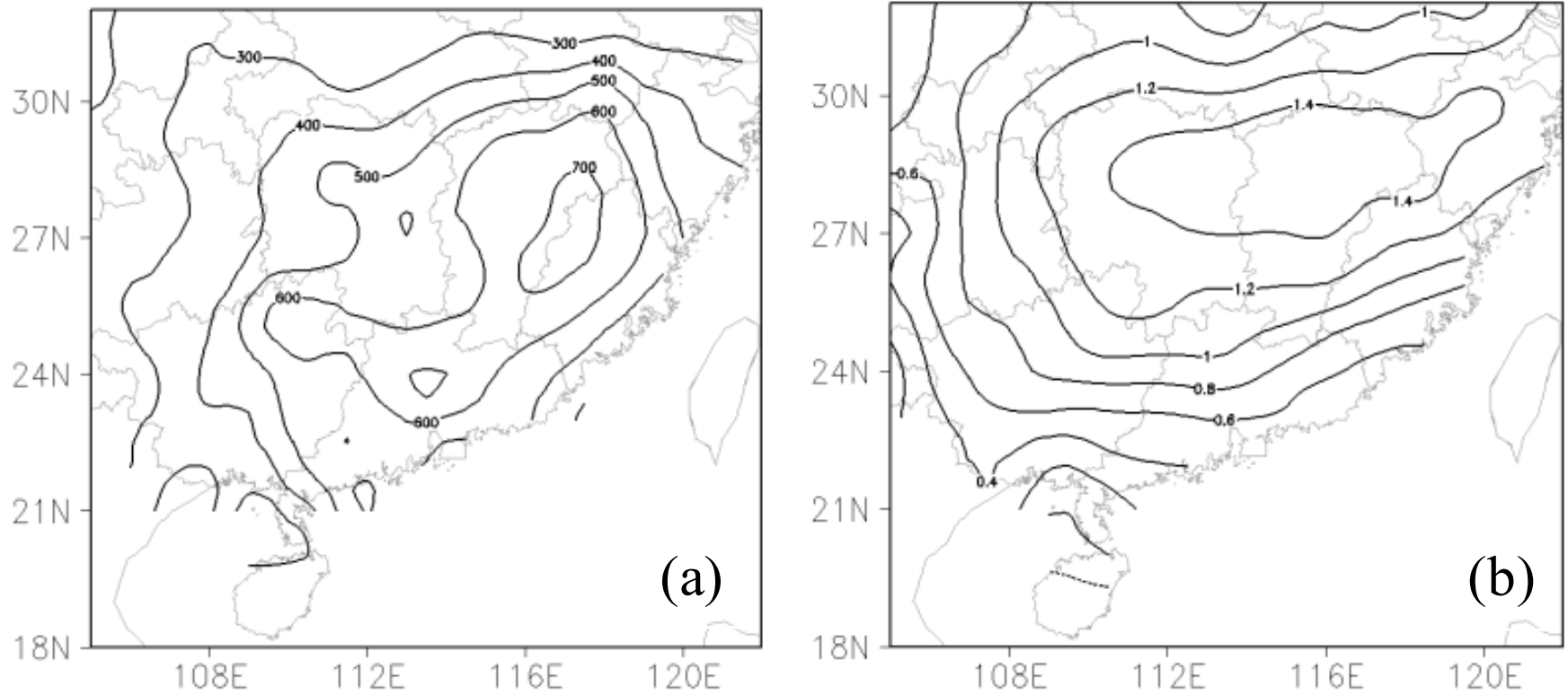


Figure 1. (a) Spatial distribution of the climatological spring (March–May) **precipitation (mm)** over Southern China for the period 1980–2008. (b) Spatial pattern of the first EOF mode (**EOF1**) for daily spring precipitation anomalies over Southern China.

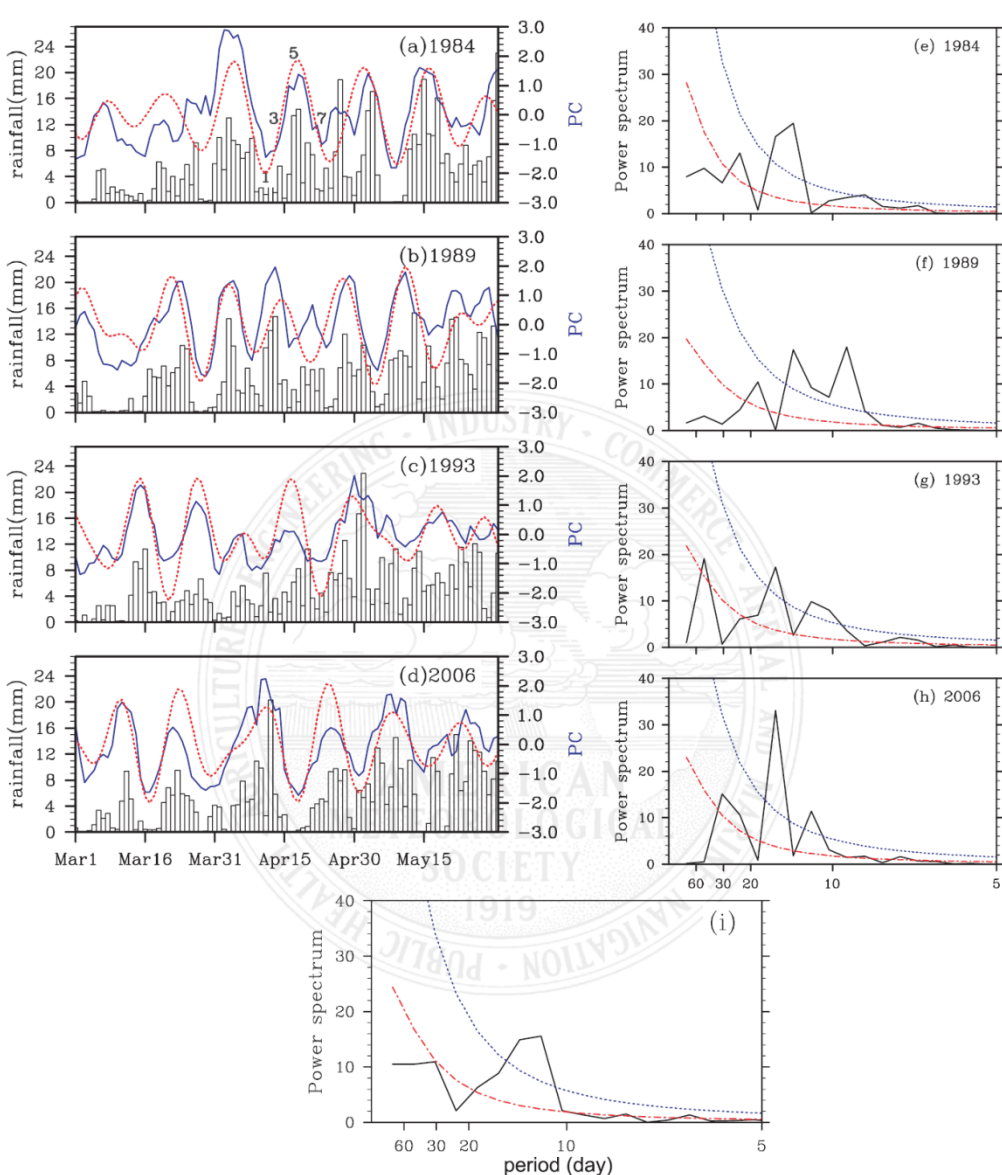


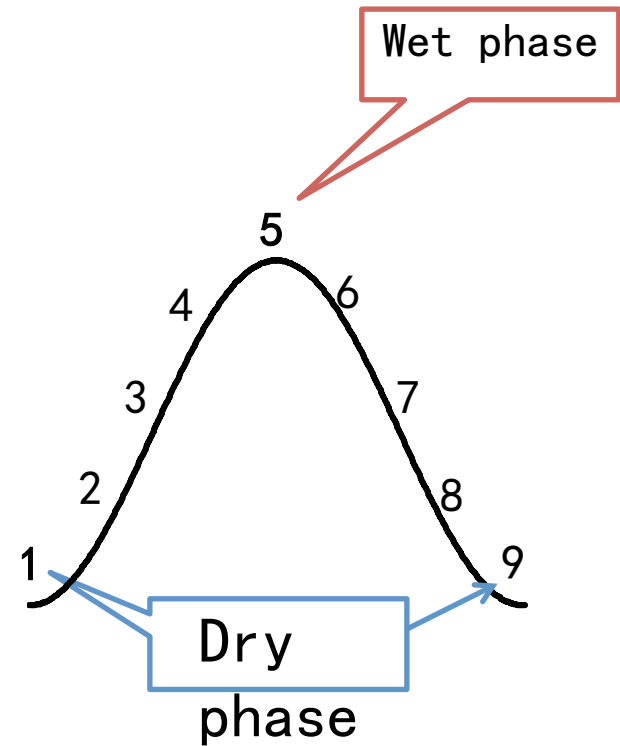
FIG. 2. Time series of daily rainfall (histogram; mm day⁻¹) averaged over southern China (18° – 32° N, 105° – 120° E), the corresponding unfiltered PC1 (blue solid curve), and the 10–20-day filtered PC1 (red dotted curve) for the typical years of (a) 1984, (b) 1989, (c) 1993, and (d) 2006. (e)–(h) The corresponding power spectrum of the unfiltered PC1 (black curve), together with the Markov red noise spectrum (red dot-dashed curve) and a posterior 95% confidence level (blue dotted curve) for the selected years and (i) the 29-yr average from 1980 to 2008. The numbers 1, 3, 5, and 7 in (a) indicate the phase of the 10–20-day oscillation.

Phase definition for the ISO/SCSR

位相合成分析方法

Lanczos滤波提取10 – 20天周期分量
作为降水ISO 指数

- 挑选标准 强ISO个例。
- 10–20天周期：46个
- 20–30天周期：38个

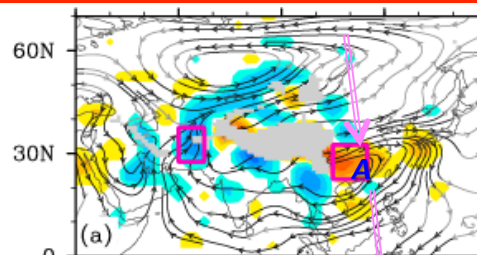


ISO振荡位相示意图

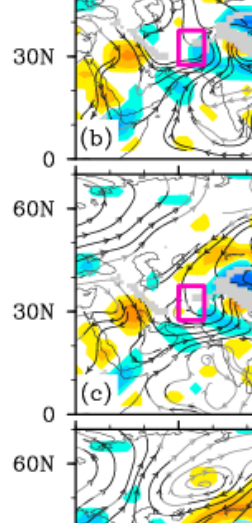
850hPa- divergence and streamfield

Dry

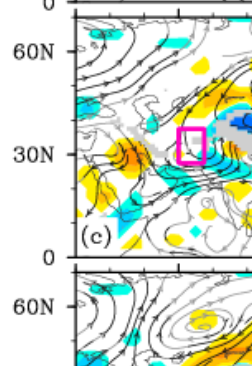
Phase 1



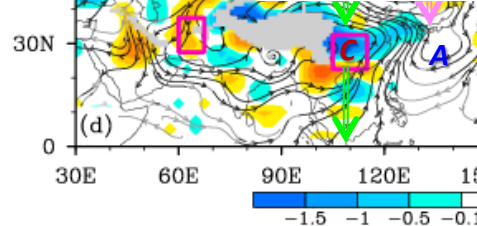
Phase 2



Phase 3

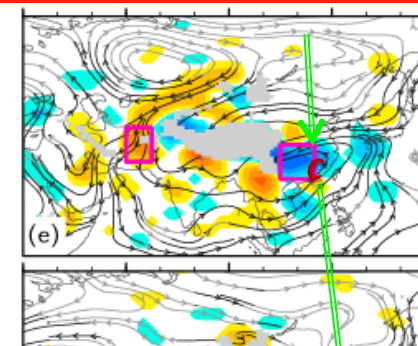


Phase 4

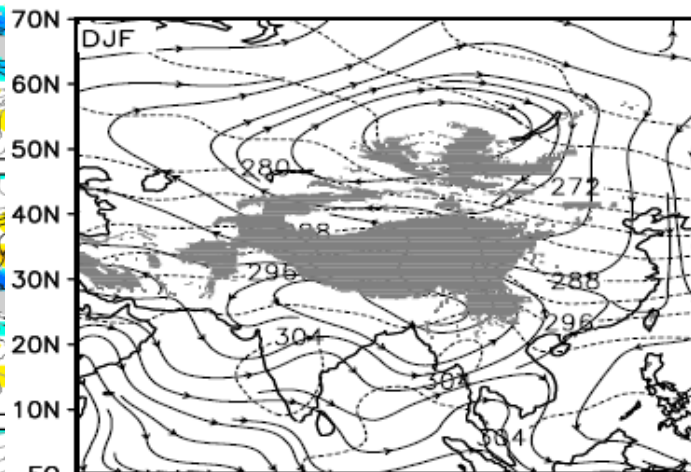


Wet

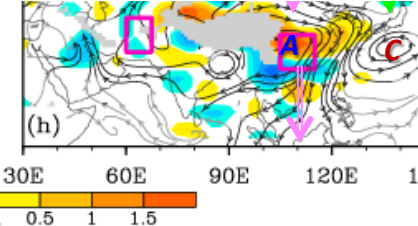
Phase 5



Phase 6



Phase 7



Phase 8

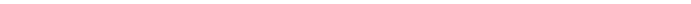


Figure 3. Composite evolution of the 10–20-day filtered 850 hPa streamline (dark streamline indicates where at least one wind component is statistically significant at the 95% confidence level) and divergence (shading, unit is 10^{-6} s^{-1} ; only shown if statistically significant at the 95% confidence level) during an ISO cycle. Phases 1–8 are shown from (a) to (h). The Tibetan Plateau with terrain above 1500 m is shaded grey. Western rectangle area (60° – 67.5° E, 27.5° – 37.5° N) to the west of the TP and eastern rectangle area (105° – 115° E, 22.5° – 32.5° N) to the east of the TP indicate the locations of the two divergence poles of the Spring Dipole Mode Index (SDMI). “A” and “C” denote, respectively, the anticyclone and cyclone centers, and arrows denote the propagation routes of the anticyclone and cyclone.

10-m streamfield and surface sensible heat flux

Dry

Wet

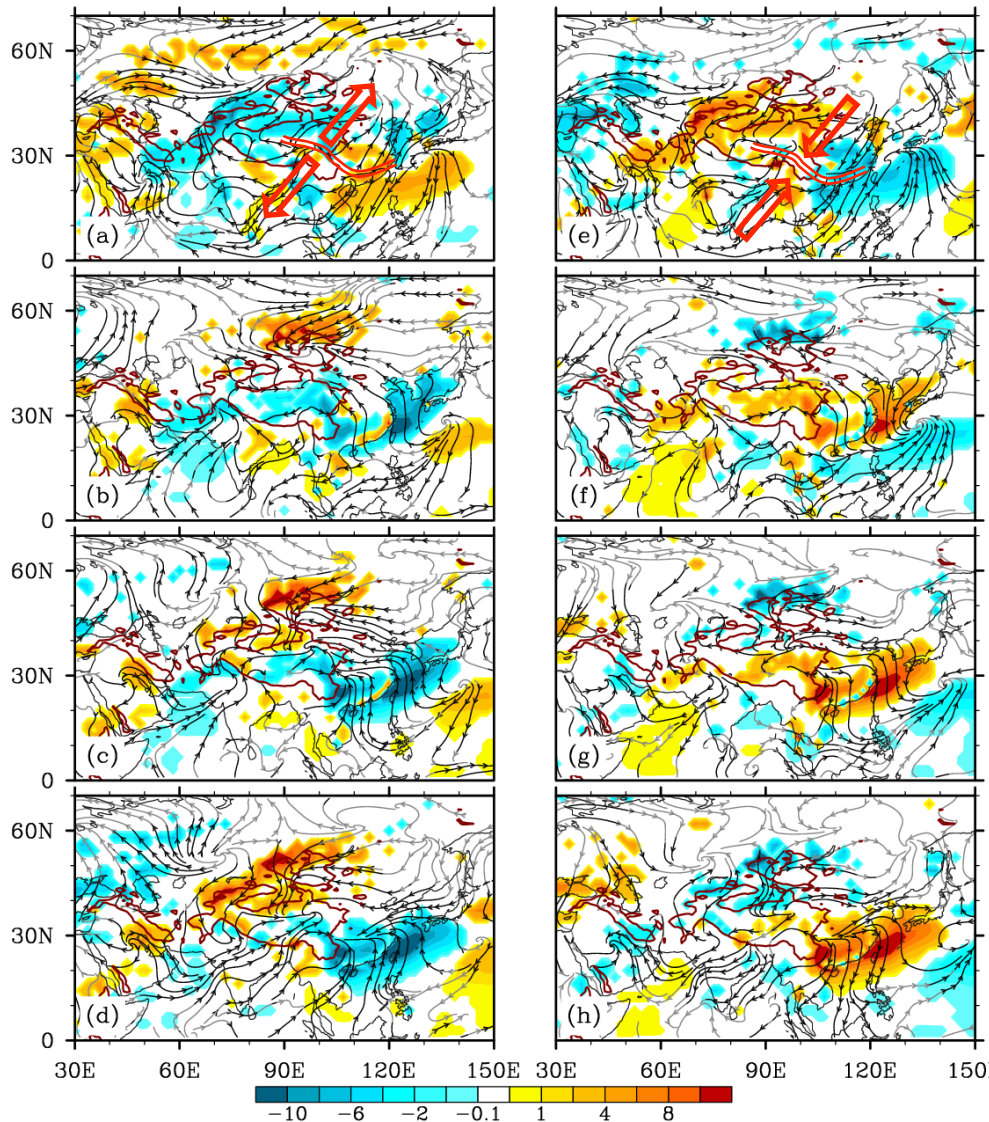
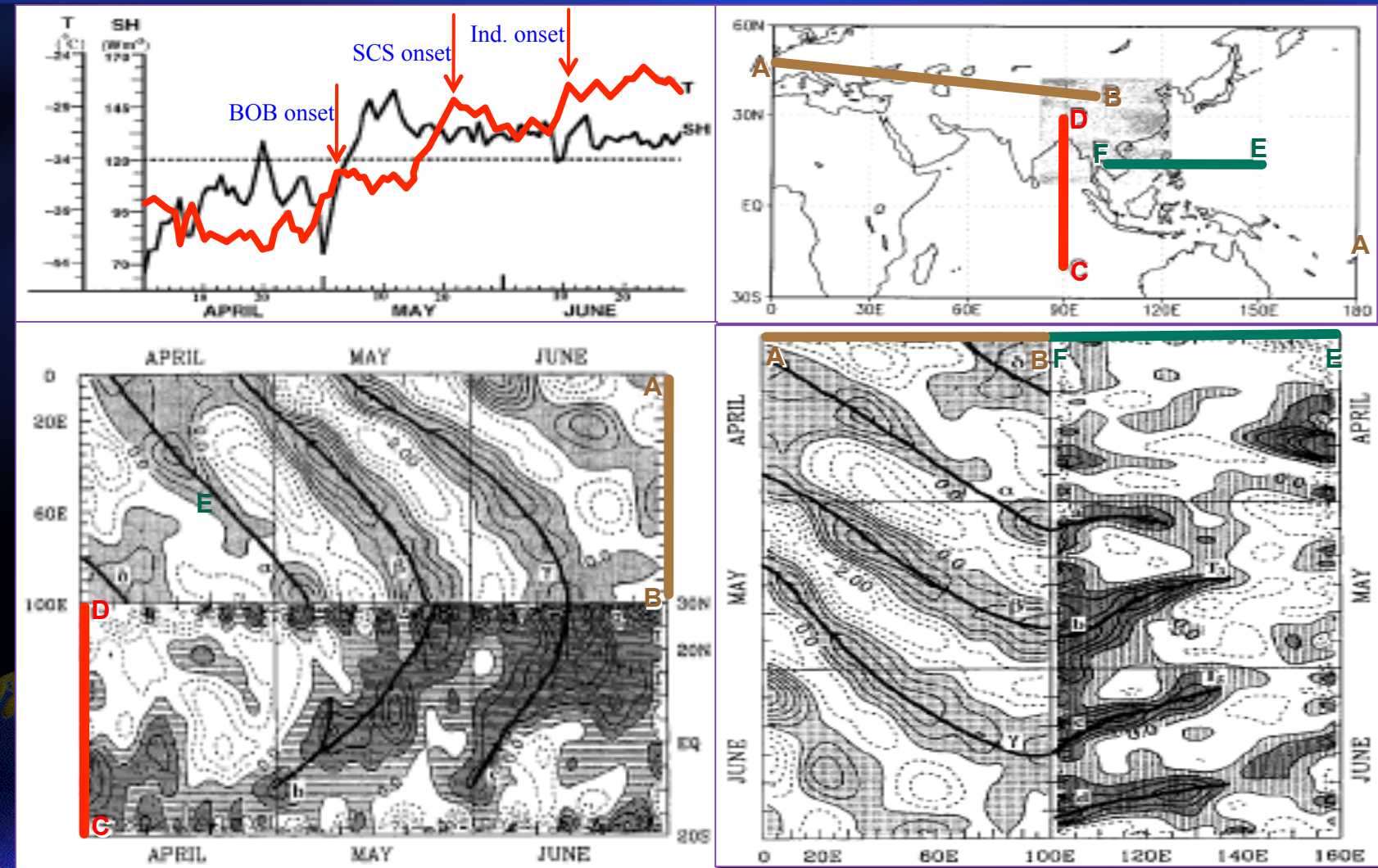


Figure 4. Same as Fig. 3, but for the 10–20-day filtered 10 m wind (vectors, m s^{-1}) and surface sensible heating flux (W m^{-2} , with shading denoting statistical significance at the 95% confidence level). The Tibetan Plateau with terrain above 1500 m is outlined by a solid curve

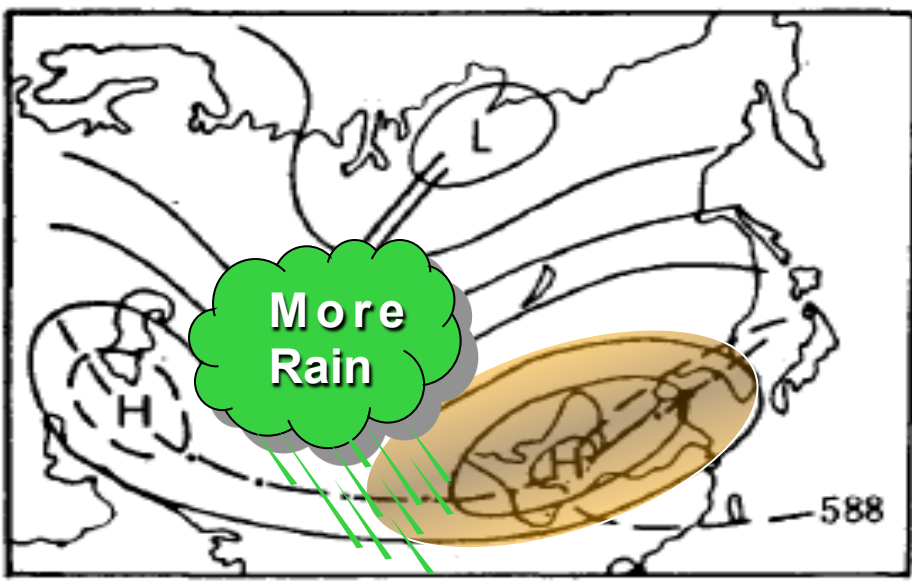
ISV: TP heating and the three – stage ASM onset



(Wu and Zhang, MWR, 1998)

夏季高原天气影响：南亚高压准双周振荡

W-mode



E-mode

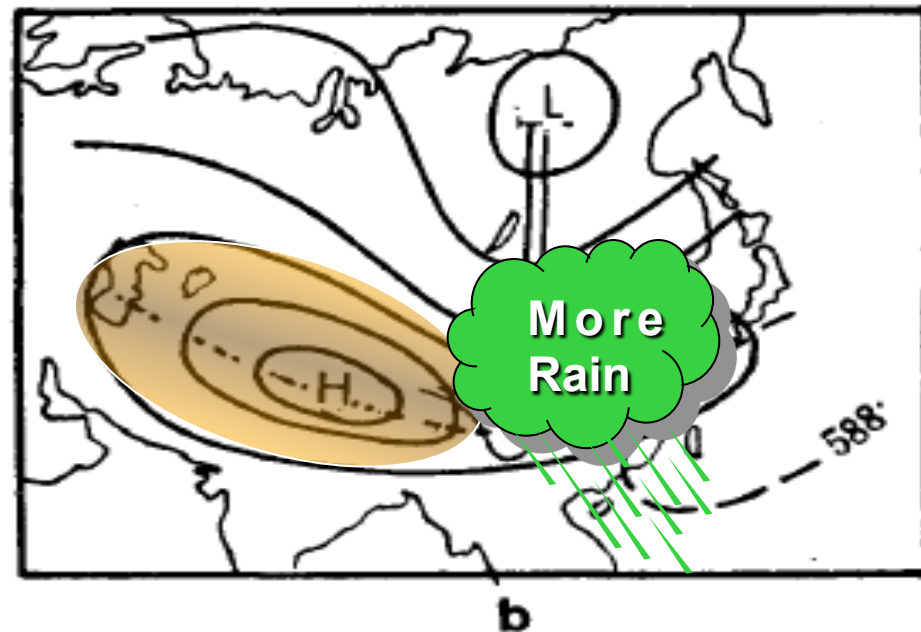


FIG. 6. Two major patterns of the Tibetan high at (a) 200 mb; and (b) 100 mb.

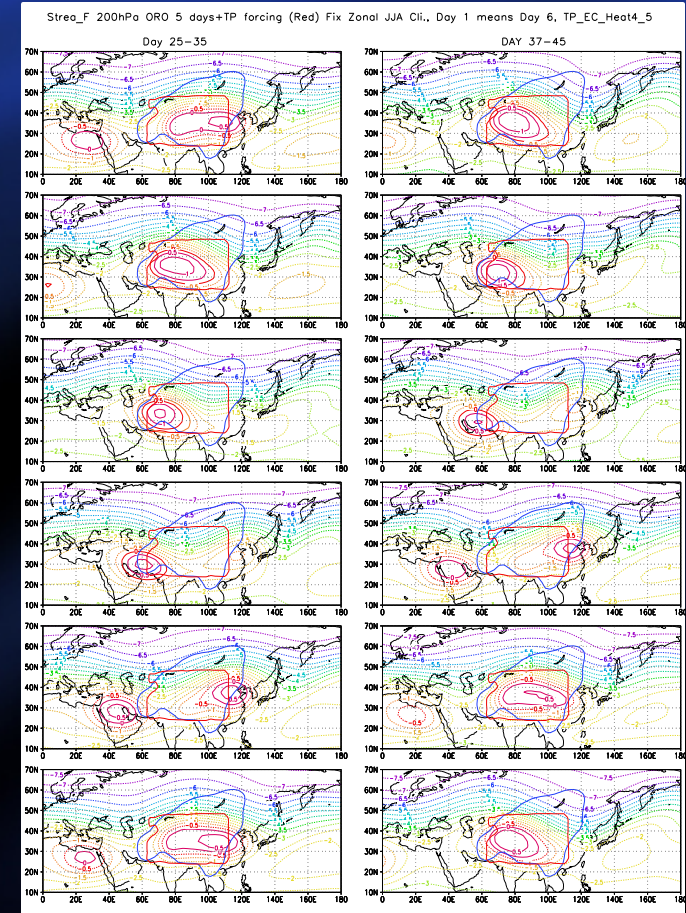
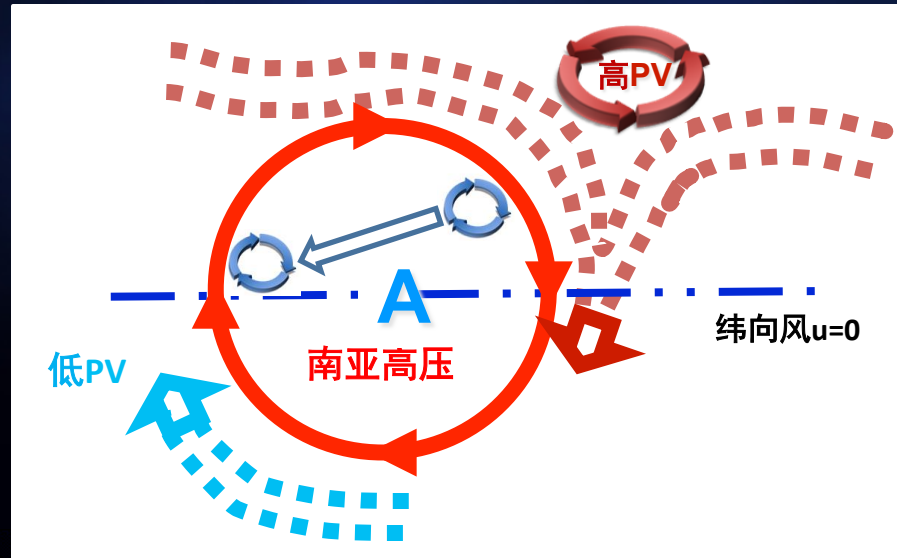
陶诗言和朱福康, 1964

加热弱:南亚高压稳定; 加热强: 不稳定

Due to PV asymmetric instability Liu等, 2007

ISV: TP summer heating and SAH oscillation

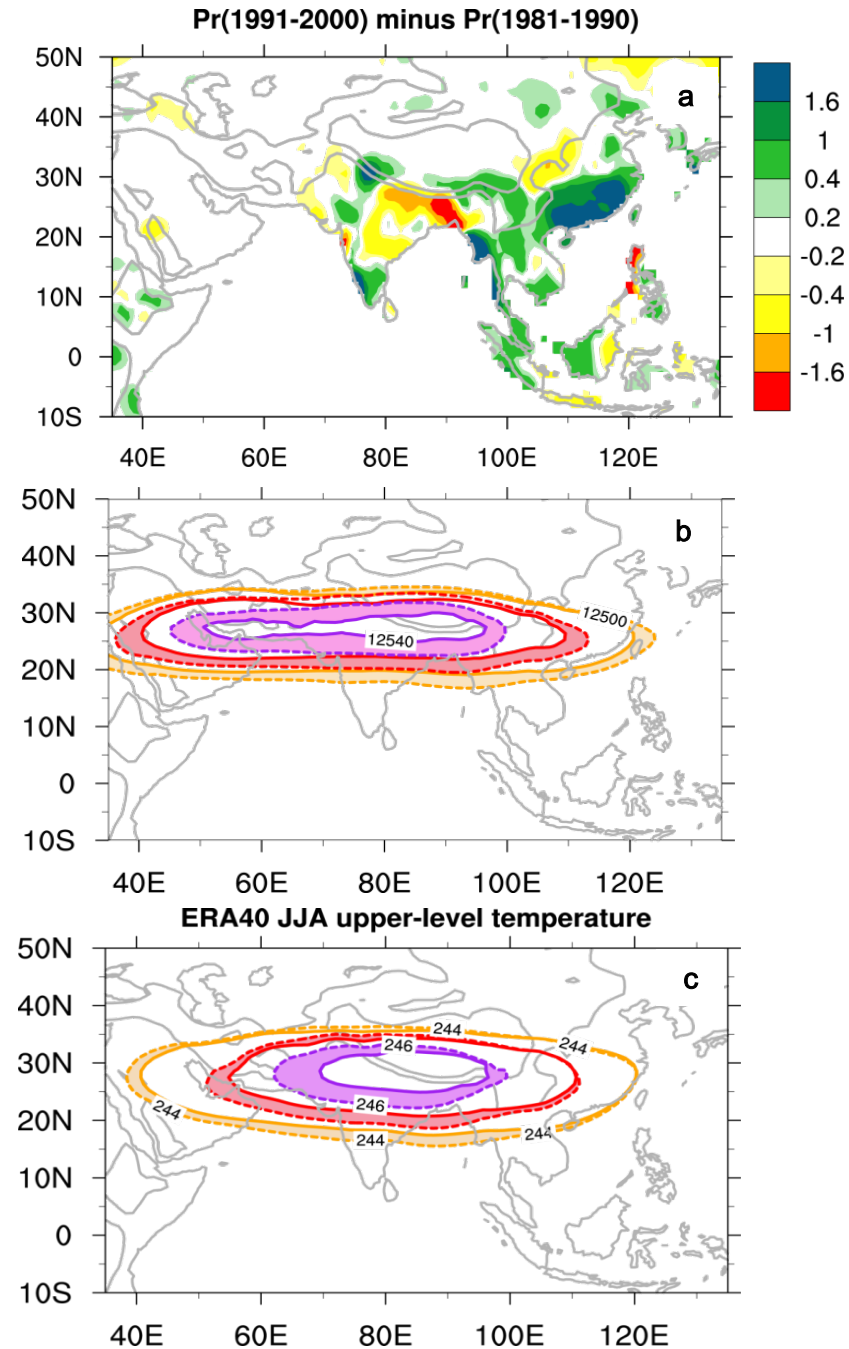
夏季青藏高原强加热能够产生准双周振荡



(Liu, Hoskins, Blackman, 2007 JMSJ)

W-E seesaw

Fig. 10 Decadal changes in JJA mean climate between the periods (1991–2000) and (1981–1990) of (a) precipitation based on the PREC/L dataset (unit: mm d^{-1}), (b) 200-hPa geopotential height (unit: gpm) and (c) the 200–400hPa mass-weighted temperature (unit: K) based on ERA40 reanalysis. The solid and dashed curves in (b) and (c) denote, respectively, the 1981–1990 and 1991–2000 means.



$$\beta v \approx (f + \zeta) \theta_z^{-1} (\partial Q / \partial z) \quad \theta_z \neq 0 \quad \vec{V} \cdot \nabla z \rightarrow 0 \quad z = -$$

$$\left\{ \begin{array}{l} \frac{\partial^2 T}{\partial x^2} \approx \gamma \frac{\partial}{\partial x} \left(\frac{\partial^2 Q}{\partial z^2} \right) \\ \\ \gamma = f(f + \zeta) H / (R \beta \theta_z), \quad \theta_z \neq 0 \end{array} \right. \quad H \cdot \text{lmp},$$

Longitude location of the SAH and UTTM

$$\left\{ \begin{array}{l} Q = Q(x) \cos \left(\frac{\pi z}{H_Q} \right) \\ \\ T = T(x) \cos \left(\frac{\pi z}{H_Q} \right) \\ \\ T(x) = T_0 \cos \left(\frac{\pi x}{L} \right) \end{array} \right.$$

$$\left\{ \begin{array}{l} T(x) = \gamma L^2 H_Q^{-2} \partial Q(x) / \partial x = \lambda \partial Q(x) / \partial x. \quad \vec{V} \cdot \nabla \zeta \rightarrow 0; \\ \\ \lambda = \gamma L^2 H_Q^{-2} \end{array} \right.$$

$$\frac{\partial v}{\partial \ln p} = -\frac{R}{f} \left(\frac{\partial T}{\partial x} \right)$$

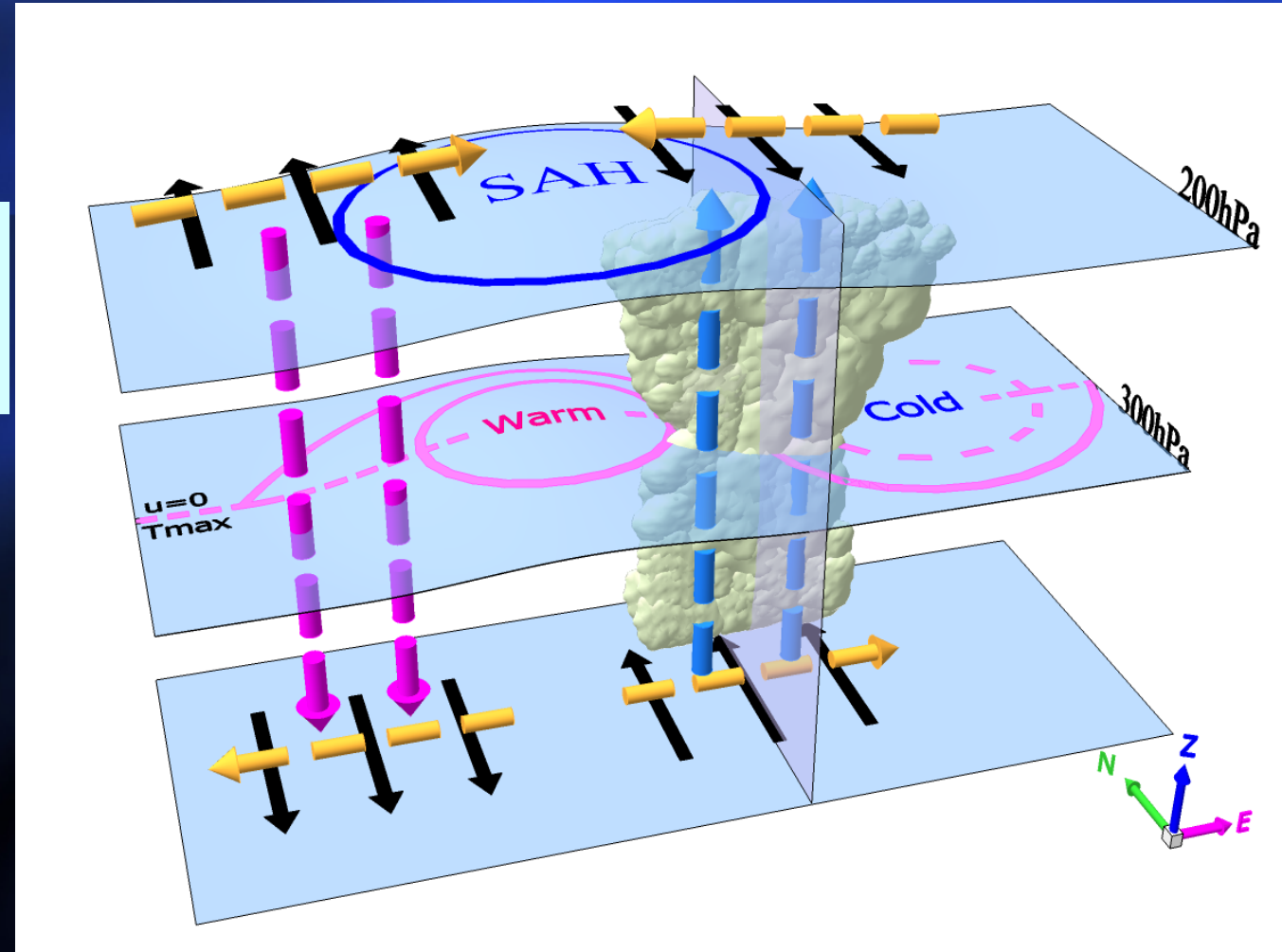


Fig. 5 Schematic diagram of the $T \cdot Q_z$ mechanism contributing to the longitudinal location of the upper-troposphere temperature maximum (UTTM): Strong monsoon convective latent heating along the subtropics (blue upward arrow) results in the local development of a vertical northerly shear (black arrow) and induces an eastward decreasing temperature gradient (orange arrow). The induced Coriolis force ($f v$, orange arrow) is in geostrophic balance with the pressure gradient force. Refer to text for details.

Longitude location of the SAH and UTTM

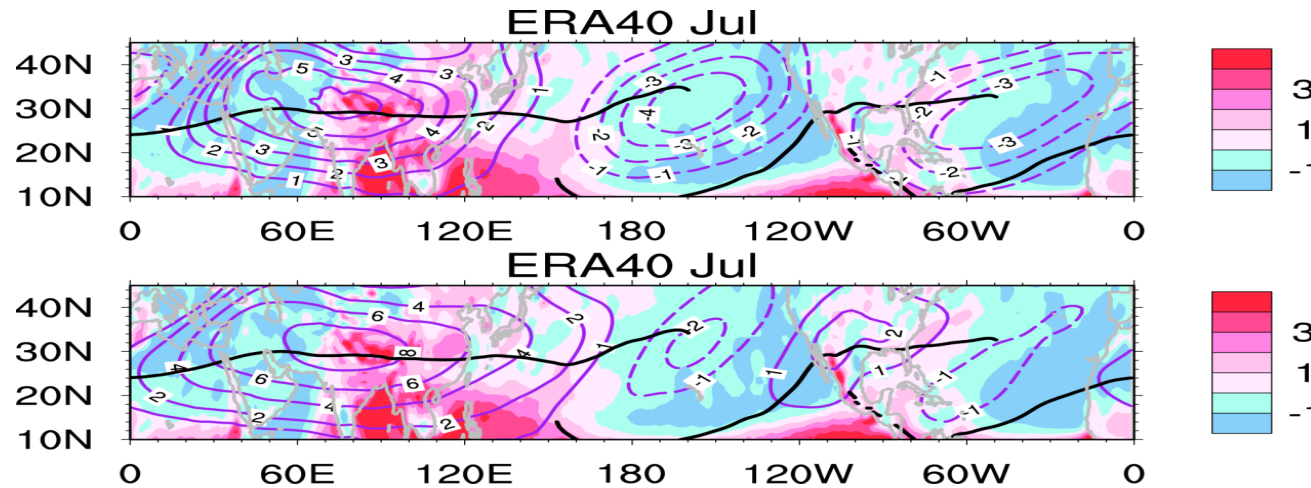


图2. 1979-1989年7月平均200-400hPa高度上的非绝热加热分布(阴影, Kd⁻¹), 以及温度对纬向平均的偏差
(a) 及对(180-360°)平均的偏差(b)的分布(兰线, K)。粗实线为副高轴线(Wu et al., 2015)

The UTTM location is determined by large-scale dynamics rather than local convection!

W-E seesaw

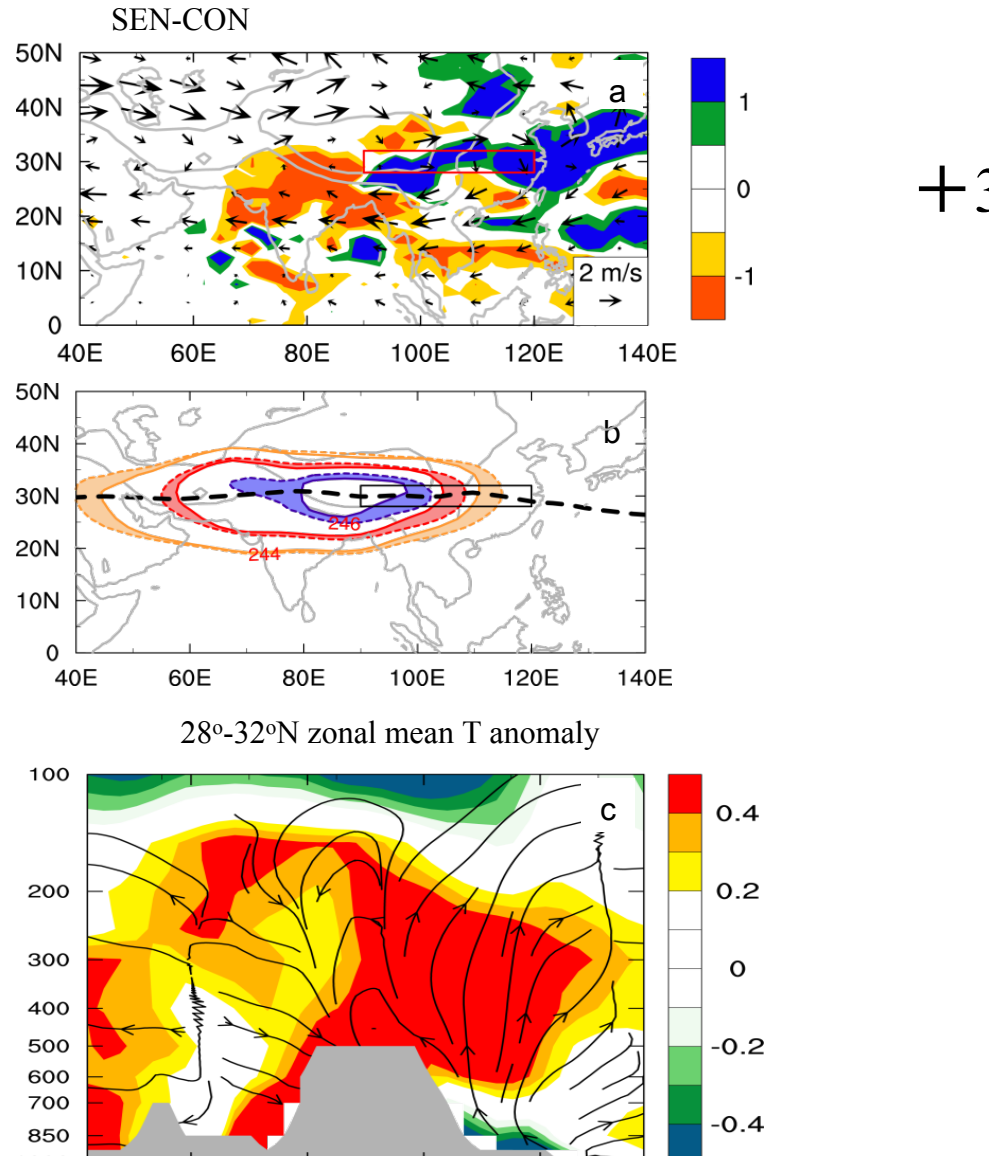


Fig. 6 Distributions of the JJA mean of (a) differences between the forcing experiment SEN and control experiment CON of rainfall (shading, unit: mm day^{-1}) and winds at 200 hPa (arrow); (b) 200–400 hPa mass-weighted temperature in the SEN run (dashed) and CON run (solid); and the differences between SEN and CON of (c) $28^{\circ}\text{--}32^{\circ}\text{N}$ zonal mean circulation (streamlines, vertical motion has been amplified by a factor of 500) and temperature (shading, unit: K); The box in (a) and (b) indicates where the extra convective heating with a maximum of 3 K day^{-1} at 500 hPa is imposed in the SEN experiment.

W-E seesaw

Fig. 7 Distributions in the PER experiment of wavelet power (a, c) and significance (b, d) for the 200-hPa geopotential height in the forcing source region S (90° – 120° E, 28° – 32° N) (a, b) and in the response region R (70° – 90° E, 28° – 32° N) (c, d); abscissa is for integration day and coordinate is for period (unit: day).

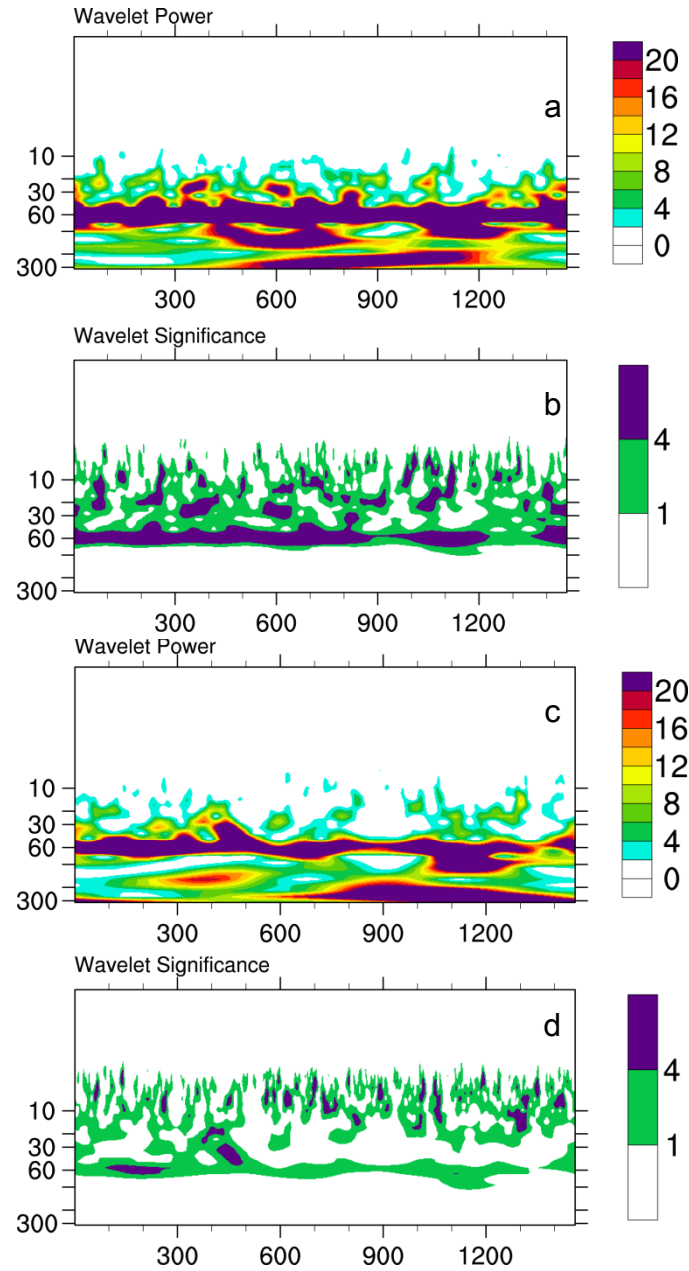


Fig. 8 Evolutions in the PER experiment of the normalized 200–500hPa mass-weighted mean heating in the forcing source region S (black solid), and the geopotential height at 200 hPa (green dashed-dotted), the 200–400 hPa mass-weighted temperature (red dashed), and pressure vertical motion at 300 hPa (blue dotted) in the response region R (a); and the corresponding time-lag correlations between the forcing in region S and those in the response region R (b). A 20-day running mean has been used on the original data to filter out high-frequency noise.

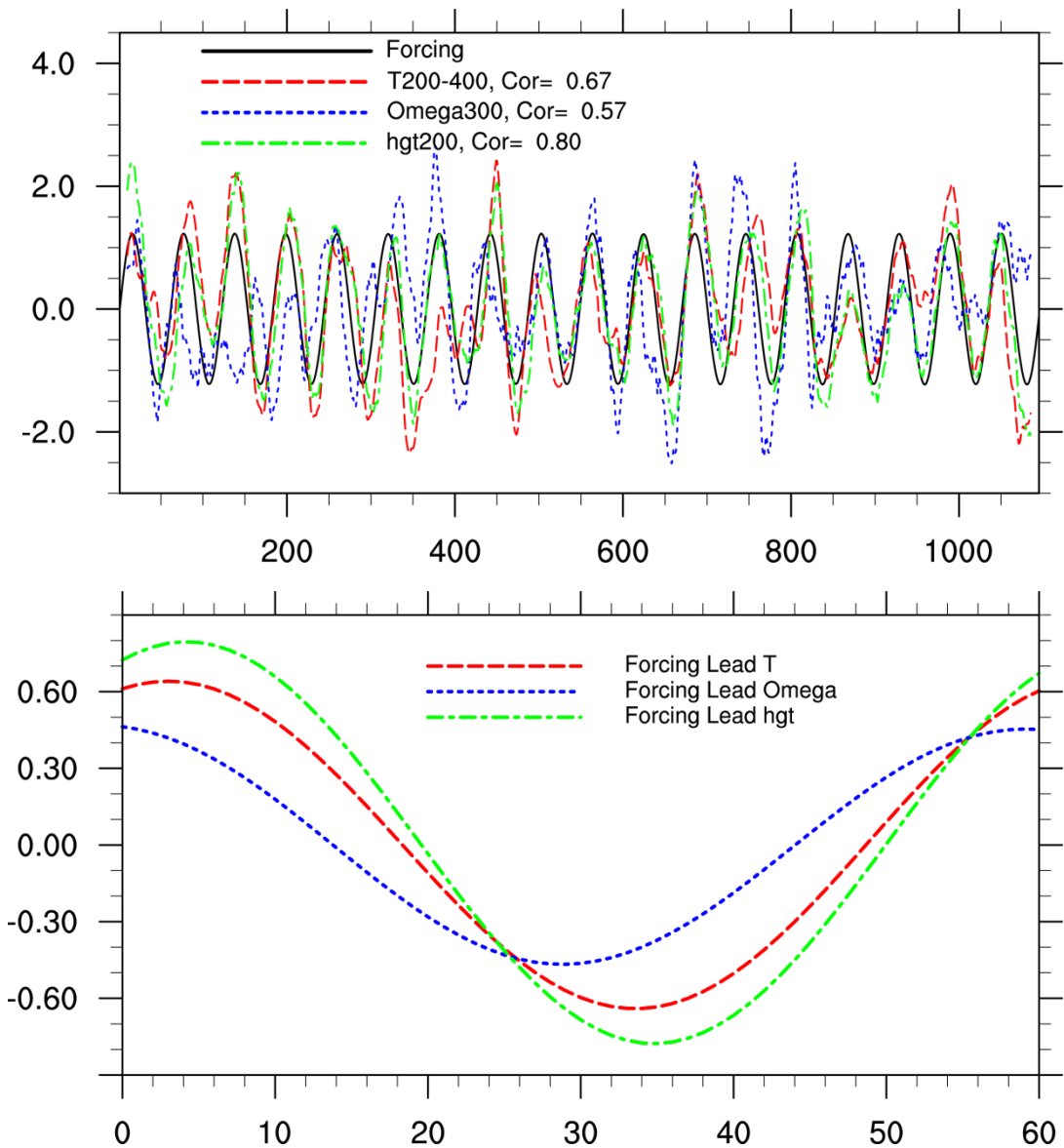


Fig. 10 Decadal changes in JJA mean climate between the periods (1991–2000) and (1981–1990) of (a) precipitation based on the PREC/L dataset (unit: mmd^{-1}), (b) 200-hPa geopotential height (unit: gpm) and (c) the 200–400hPa mass-weighted temperature (unit: K) based on ERA40 reanalysis. The solid and dashed curves in (b) and (c) denote, respectively, the 1981–1990 and 1991–2000 means.

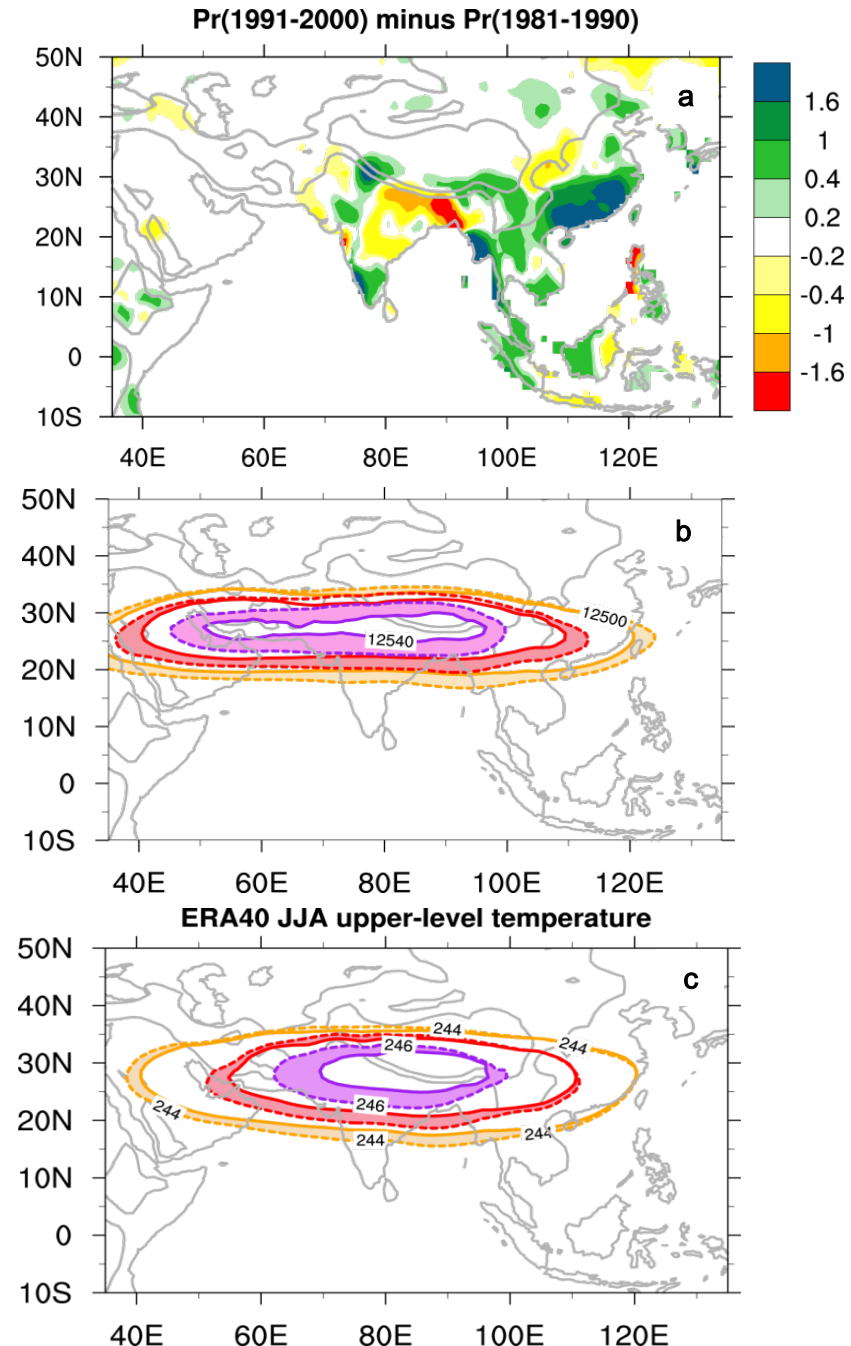
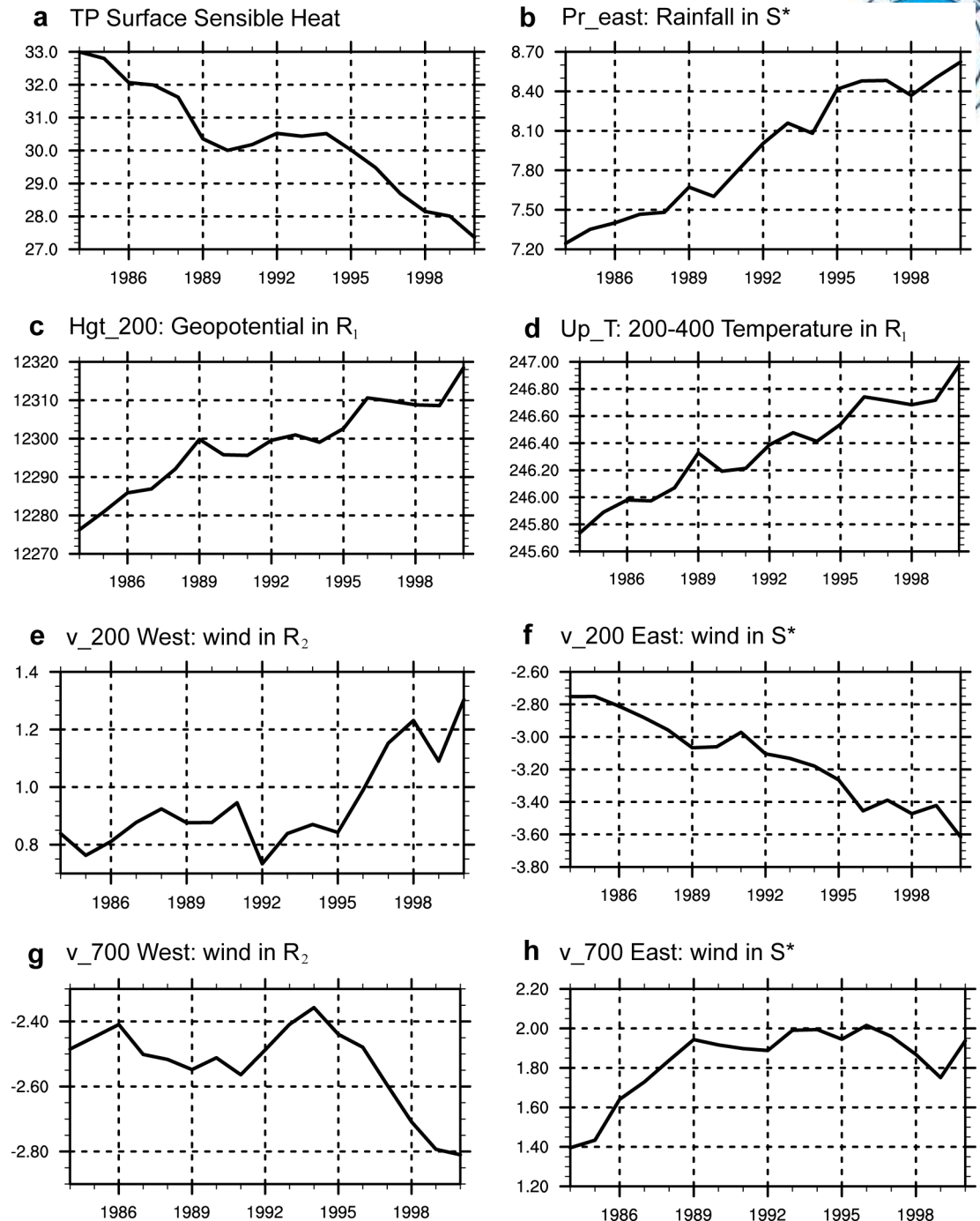
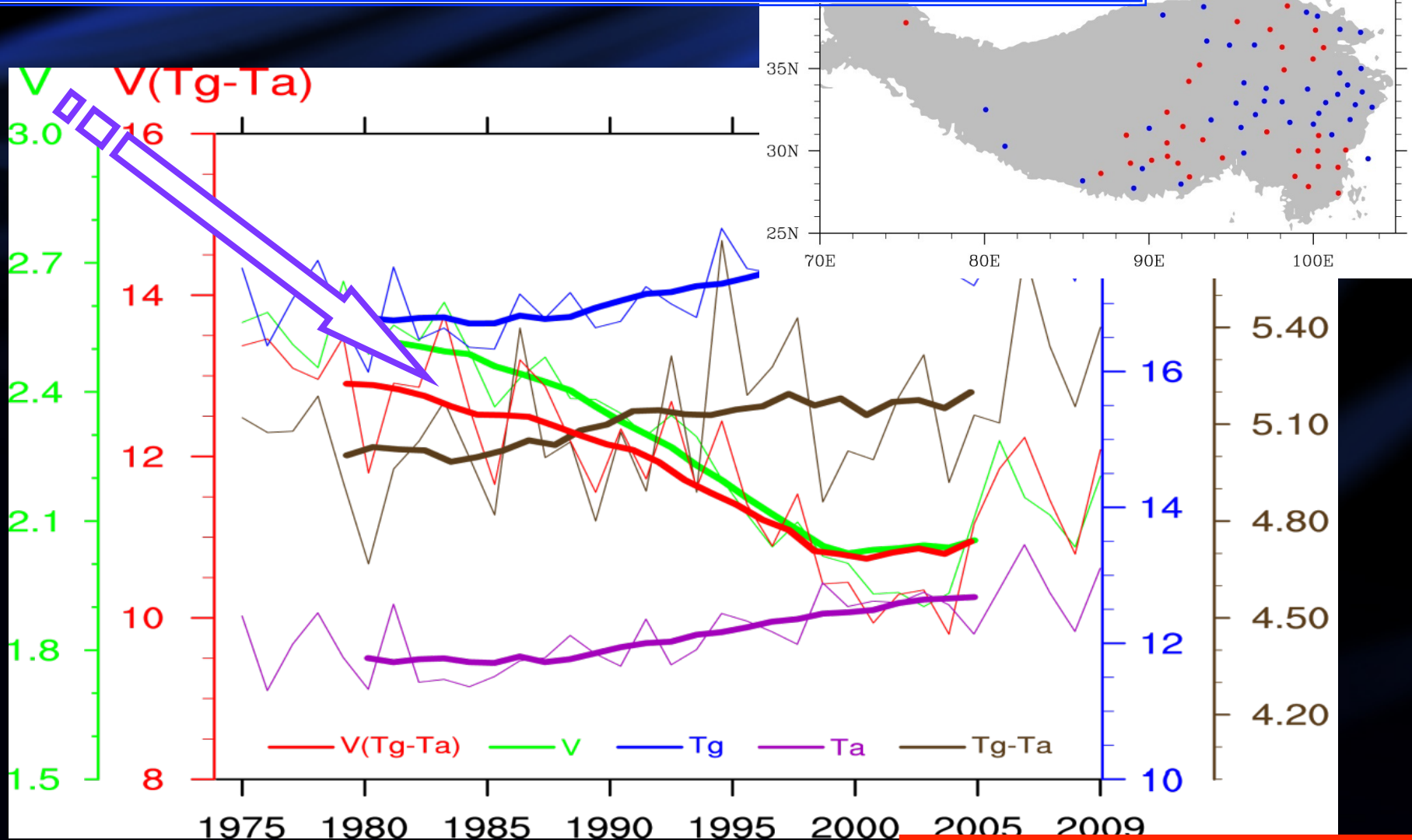


Fig. 11 Evolution from 1984 to 2000 of the JJA mean based on the ERA40 reanalysis of (a) surface sensible heat flux on the Tibetan Plateau region ($80^{\circ}\text{--}100^{\circ}\text{E}$, $26^{\circ}\text{--}36^{\circ}\text{N}$ unit: W m^{-2}), (b) precipitation in the forcing source region S^* (Pr_{east} : $90^{\circ}\text{--}120^{\circ}\text{E}$, $24^{\circ}\text{--}28^{\circ}\text{N}$, unit: mm d^{-1}), (c) 200 hPa geopotential height in the response region R_1 (hgt_200 : $70^{\circ}\text{--}90^{\circ}\text{E}$, $24^{\circ}\text{--}28^{\circ}\text{N}$ unit: dgpm), (d) 200–400 hPa mass-weighted temperature in R_1 (Up_T , unit: K), 200 hPa meridional wind (e) in the response region R_2 (v_{200} West: $50^{\circ}\text{--}80^{\circ}\text{E}$, $24^{\circ}\text{--}28^{\circ}\text{N}$) and (f) in S^* (v_{200} East, unit: ms^{-1}), and 700 hPa meridional wind (g) in R_2 (v_{700} West) and (h) in S^* (v_{700} East, unit: ms^{-1}).



(1) A weakening trend in the TP forcing in spring and summer from station data

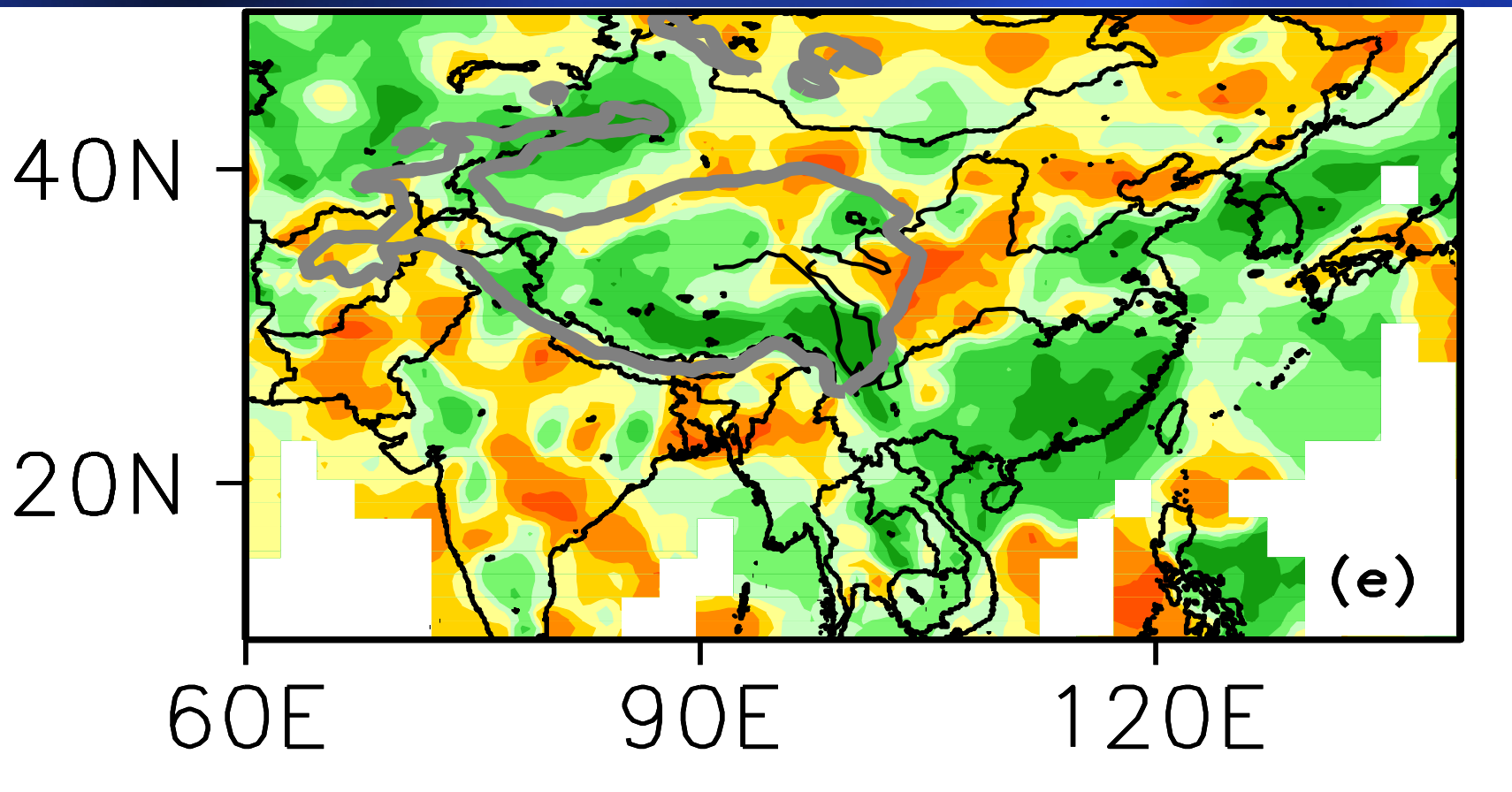


Mean over the TP, JJA

Liu et al. Cli. Dyn 2012

$$\frac{\Delta SH}{SH} = \frac{\Delta V}{V} + \frac{\Delta(T_g - T_a)}{T_g - T_a} \approx \frac{\Delta V}{V}$$

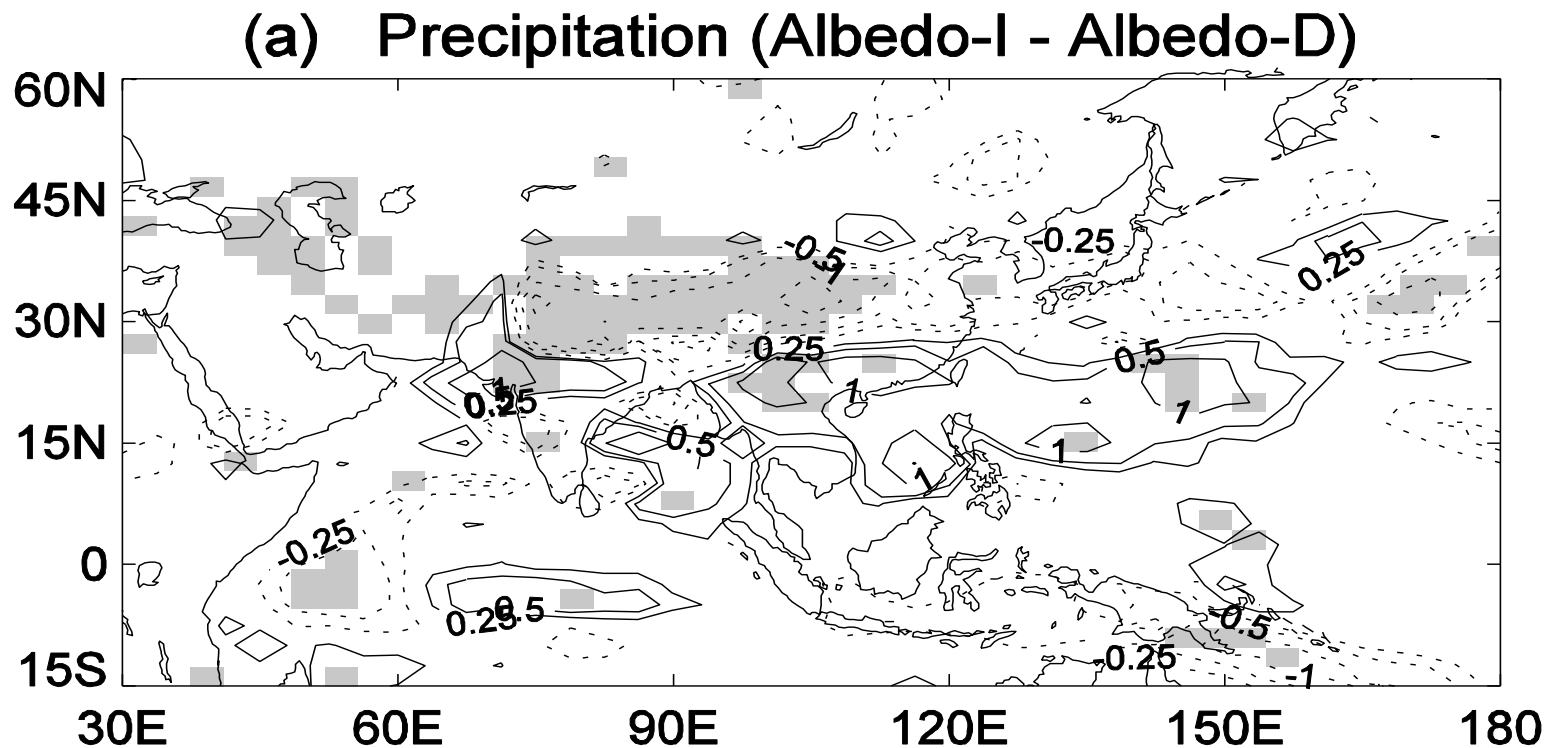
N-S seesaw



Correlation: weaker TP heating corresponds to more rain (green) in Southern China and less rain (brown) in Northern China

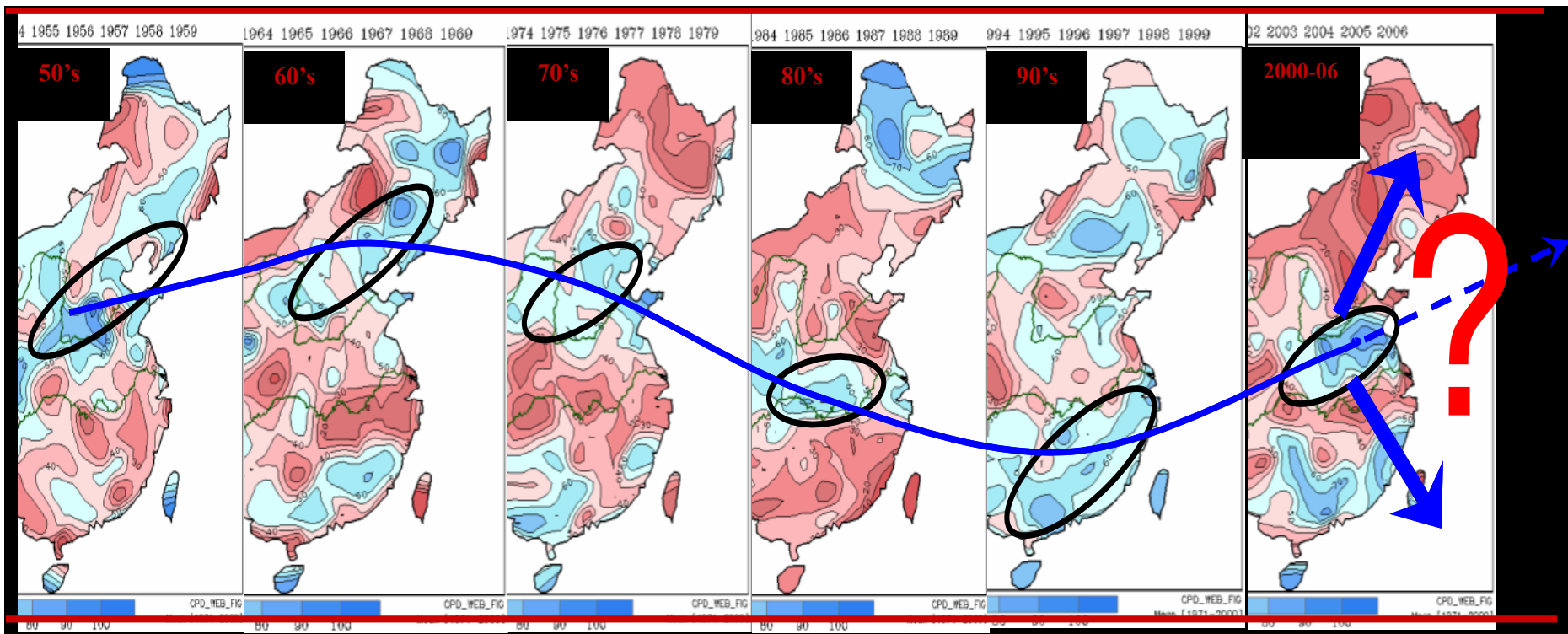
N-S seesaw

Response

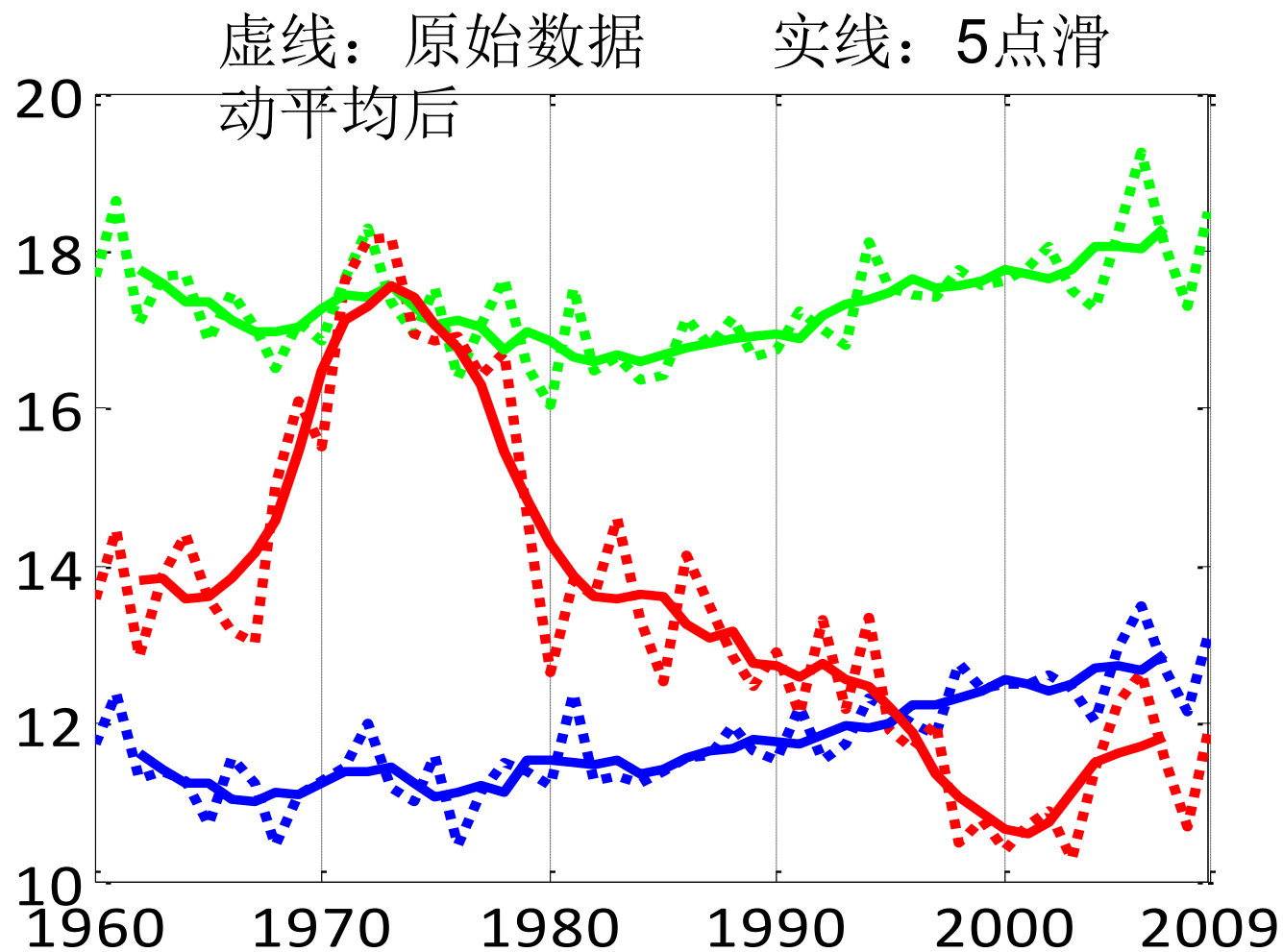


Less rain in north
More rain in South

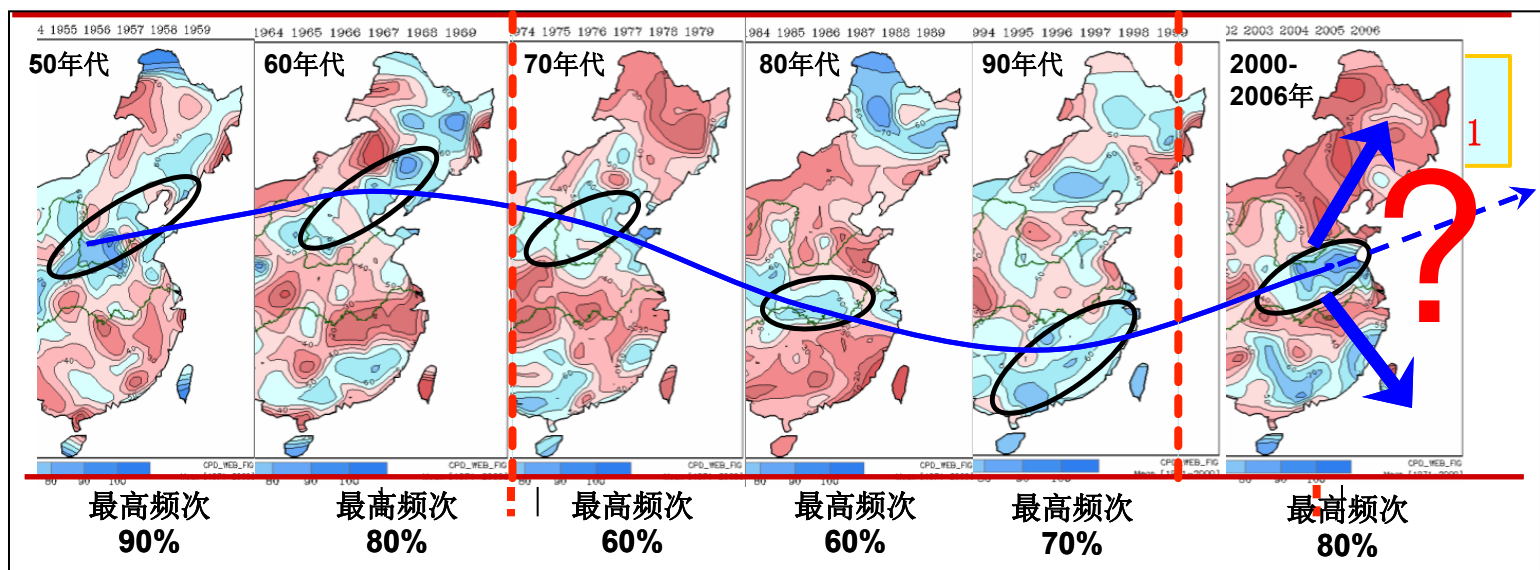
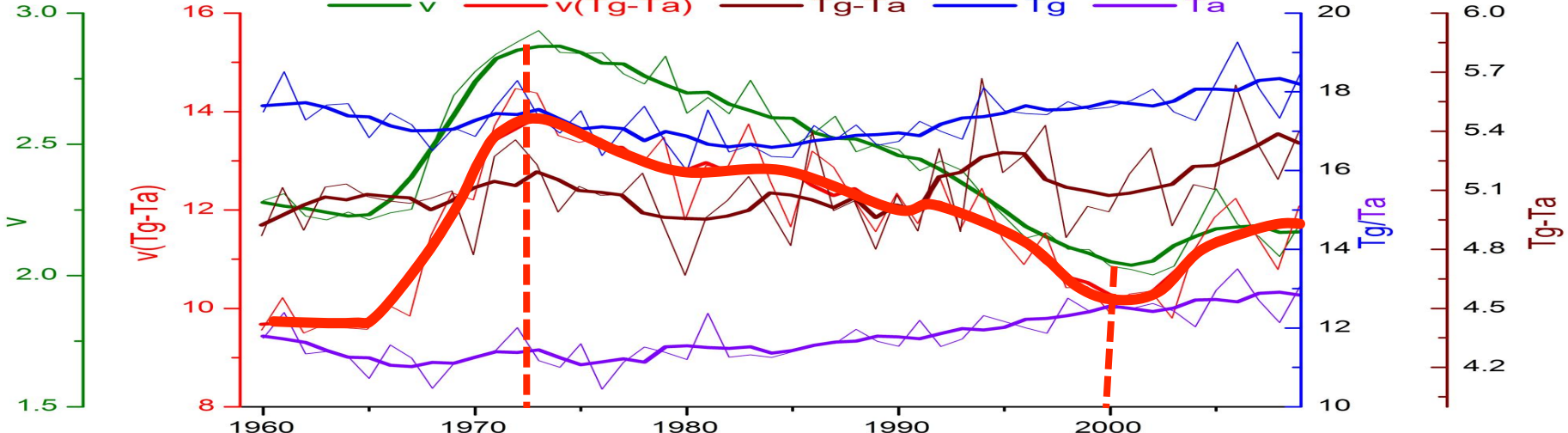
中国未来极端降水事件？



Inter-decadal variation of summertime rainfall anomaly over E China
From Dong et al. 2009



绿色: Tg 蓝色: Ta 红色: $(Tg-Ta)V$



$$PSH=V(Tg-Ta)$$

Summary- III

Weakening of sensible heating over the TP results in weakening of near-surface cyclonic circulation. Consequently, the convergence of water vapor transport is confined to South China, contributes to “wet in south and dry in north.”

Outline

1

Variability of the ASM



2

Dynamics of ASM onset

亚洲夏季风爆发动力学

3

Evolution of the ASM onset

亚洲夏季风爆发过程

4

ENSO and ASM Onset

ENSO和亚洲夏季风爆发

5

Summary 结论



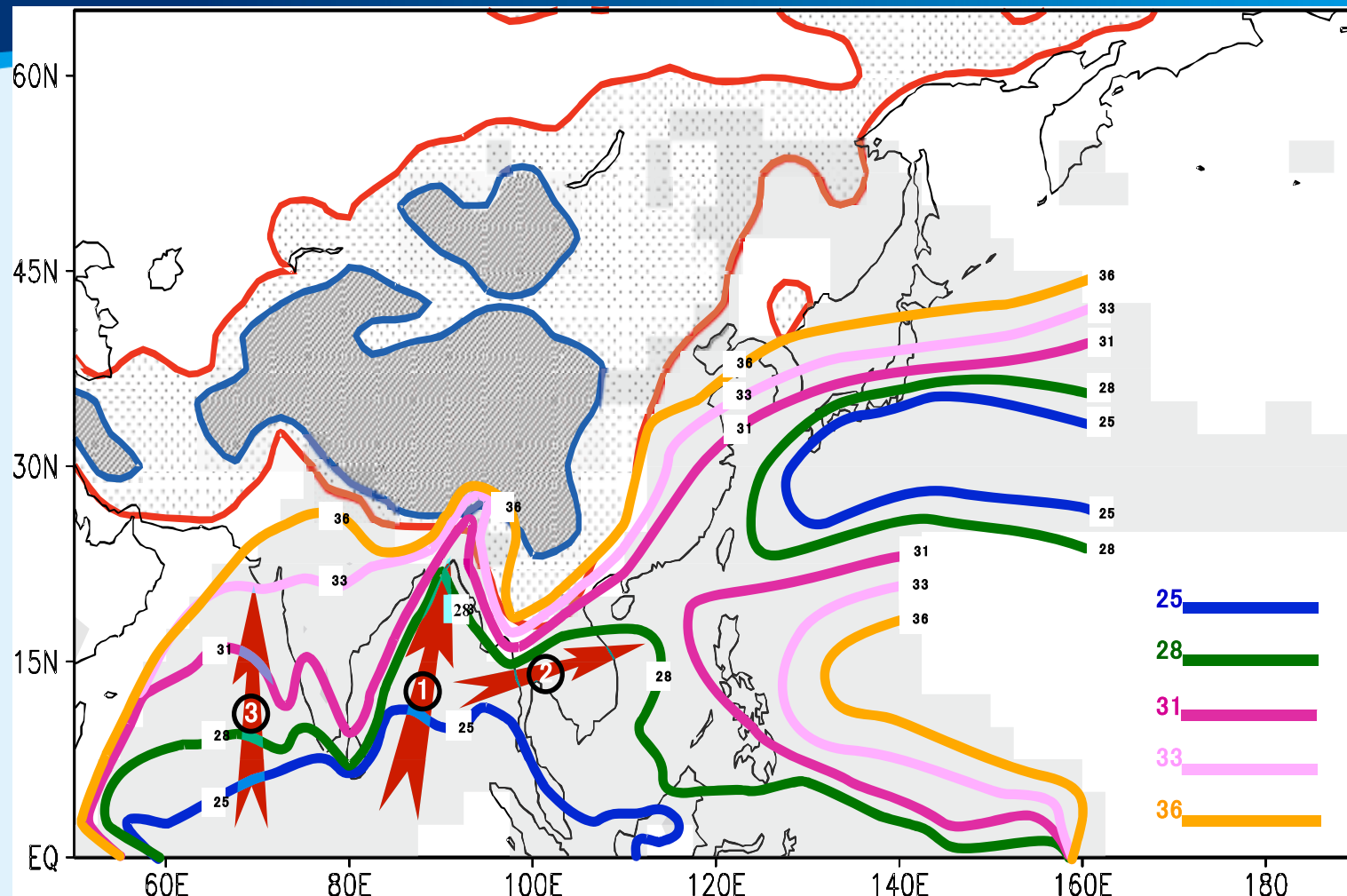


Fig. 4 Climate-mean Pentad-isochrones indicating the evolution of the Asian summer monsoon onset, Unit: pentad

Wu and Zhang, MWR, 1998



Upper-lower troposphere coupling

Upper
troposphere

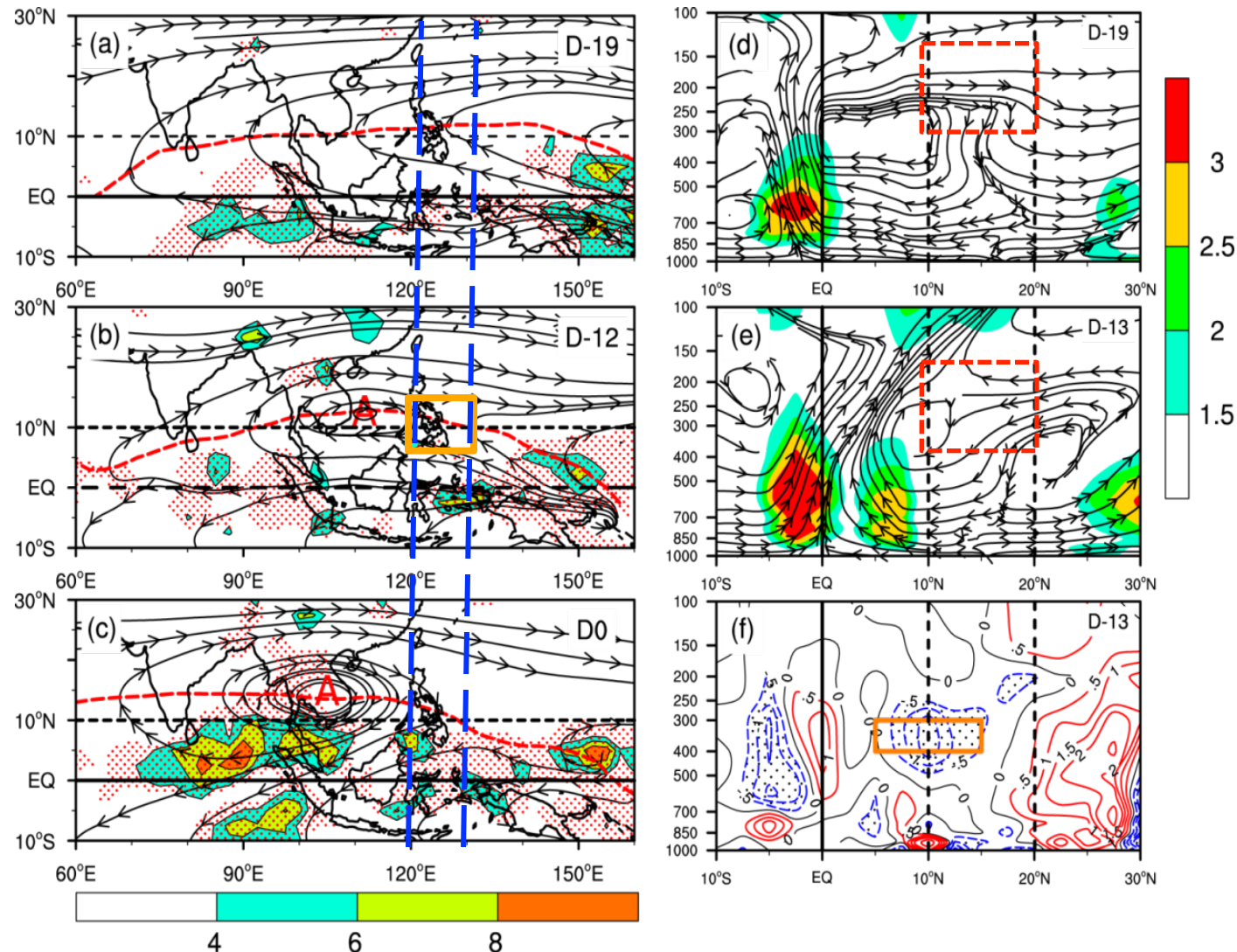
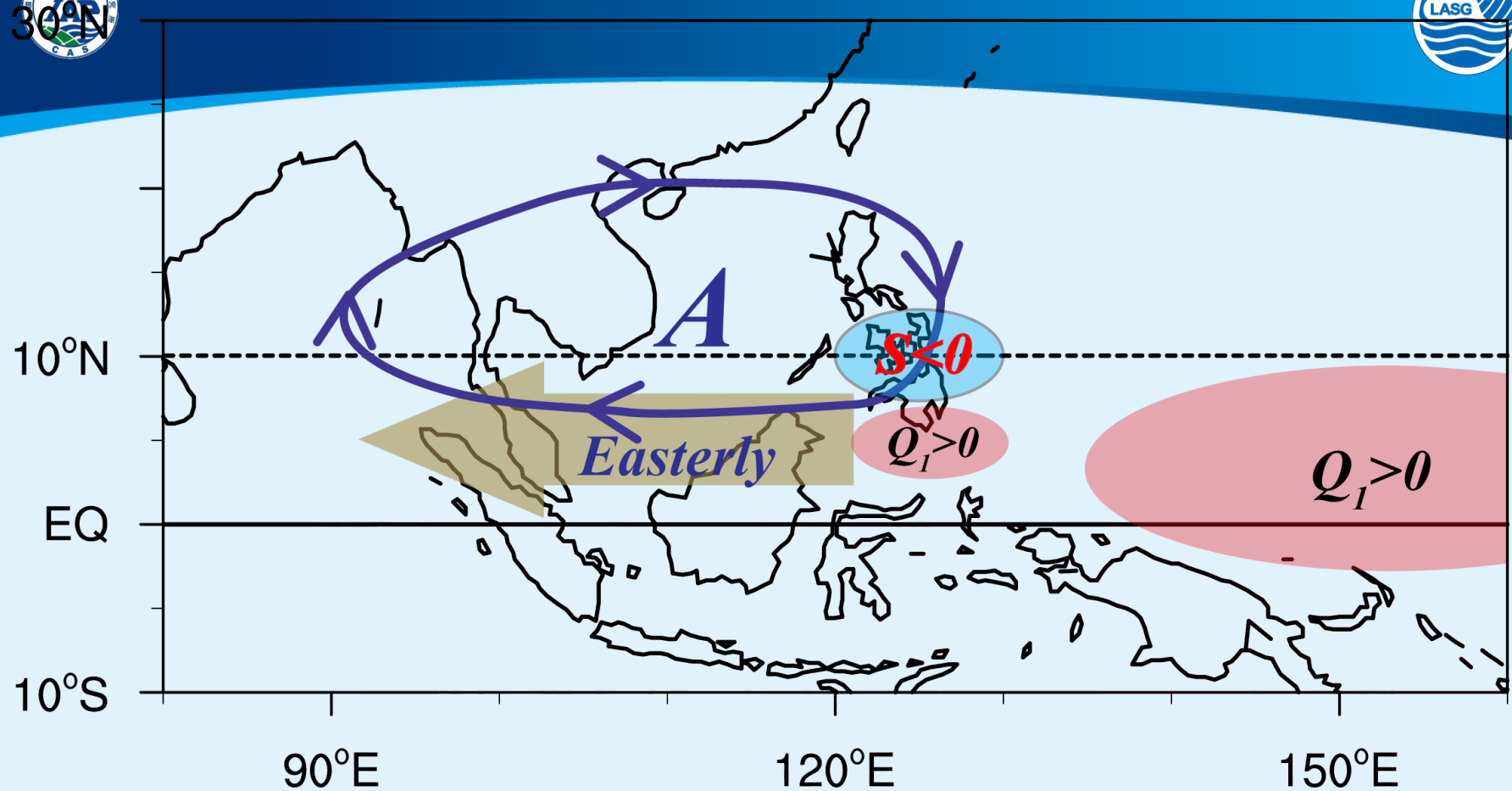


Fig. 8 Streamline and divergent field (shaded, units: 10^{-6} s^{-1}) at 150hPa, and the diabatic heating averaged from 500hPa to 200hPa (red stipple denotes greater than 1.5 K day^{-1}) during the BOB summer monsoon onset period on (a): D-19, (b): D-12, c: (D0); the Pressure–latitude cross section (averaged over $120^\circ\text{--}130^\circ\text{E}$) of Q_1 (shading, units: K day^{-1}) and meridional circulation on (d) D-19 and (e) D-13; and (f) vorticity source S on D-13 (interval is $0.5 \times 10^{-11} \text{ s}^{-2}$, values greater than -0.5 are stippled). “A” and the red dash line in (a) to (c) denote, respectively the anticyclone center and the ridgeline. The orange boxes in (f) denotes the area of maximum S over Philippines. (reproduced from Liu et al., 2012)



Schematic diagram presenting the mechanism responsible for the SAH (marked by “A”) formation: persistent convective diabatic heating in spring over the south Philippines produces a sustained negative vorticity source over the Philippines, and the South Asian High is generated as a Gill-type atmospheric response to the negative forcing source. The marked area over the equatorial west Pacific denotes the diabatic heating which is isolated from the one over the south Philippines.

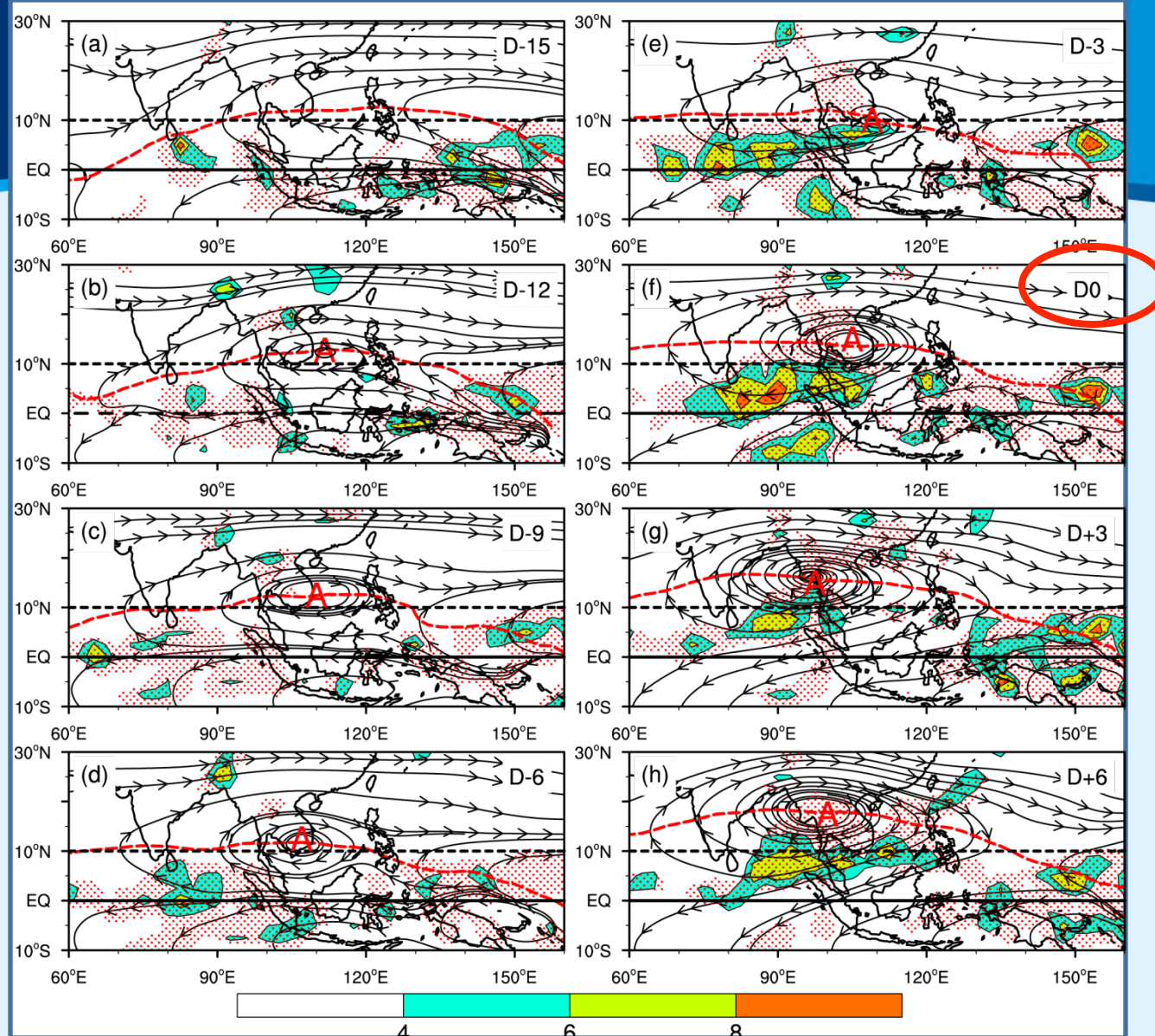


Fig. 1 Daily evolution of **150hPa streamline** and **divergent field** (shaded, units: 10^{-6} s^{-1}) , and **the diabatic heating** averaged from 500hPa to 200hPa (red stipple denotes greater than 1.5 K day^{-1}) during the BOB summer monsoon onset period (a: D-15, b: D-12, c: D-9, d: D-6, e: D-3, f: D0, g: D+3, h: D+6). “A” denotes the anticyclone center, the ridgeline is plotted by the red dash line.



Upper-lower troposphere coupling



Lower troposphere

- BOB monsoon onset
- Indian monsoon onset

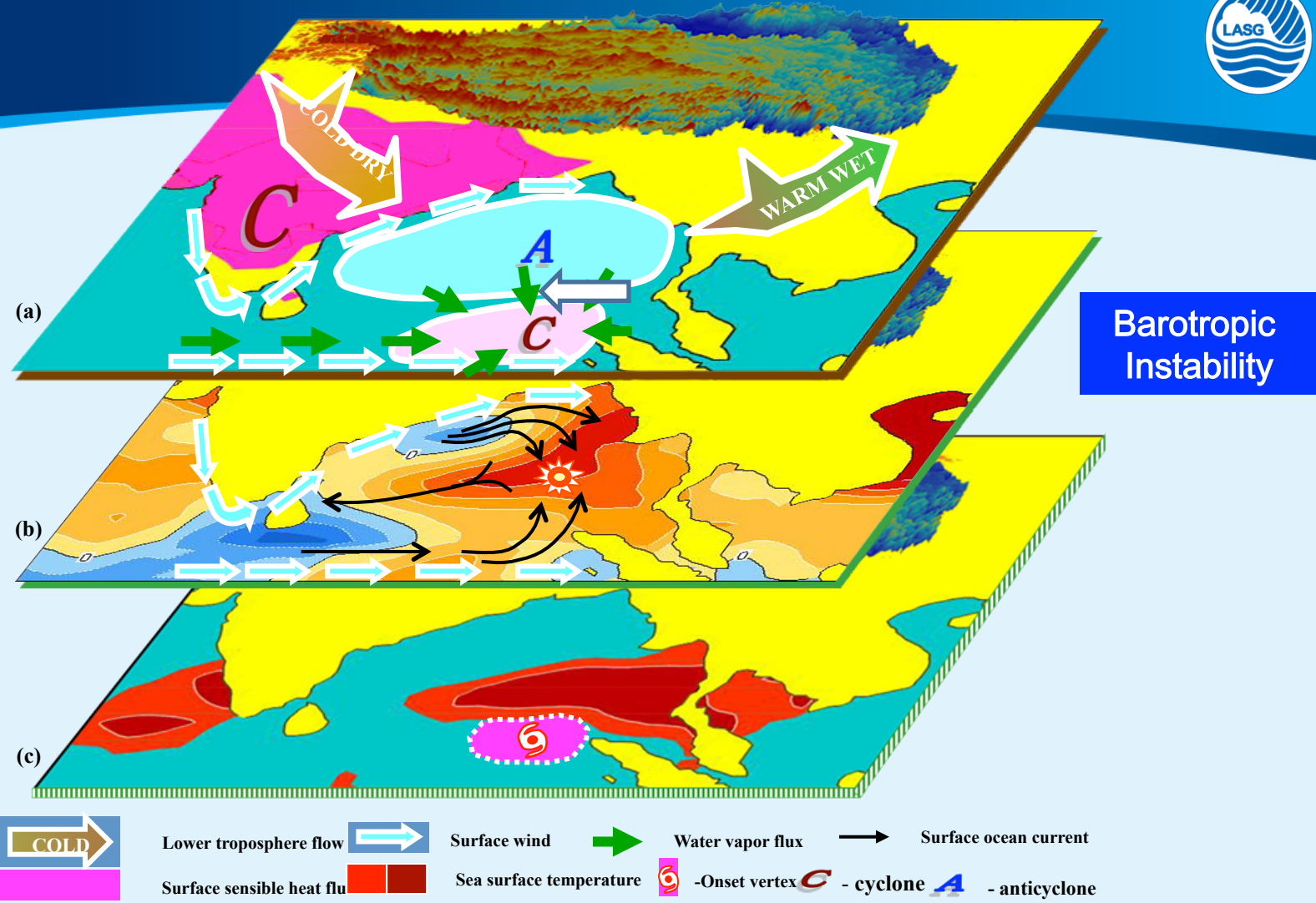


Fig. 7 Schematic diagram showing the formation of the BOB monsoon onset vortex as a consequence of *in situ* air-sea interaction modulated by the land-sea thermal contrast in South Asia and Tibetan Plateau forcing in spring. (adopted from Wu et al., 2012a)

图7 春季在青藏高原强迫和南亚海陆热力对比共同作用下(a), 孟加拉湾暖池形成(b)和季风爆发涡旋激发(c)的示意图, 详见正文。引自Wu等(2012a)

Outline

1

Introduction 引言

2

Dynamics of ASM onset

亚洲夏季风爆发动力学

3

Evolution of the ASM onset

亚洲夏季风爆发过程

4

ENSO and ASM Onset

ENSO和亚洲夏季风爆发

5

Summary 结论



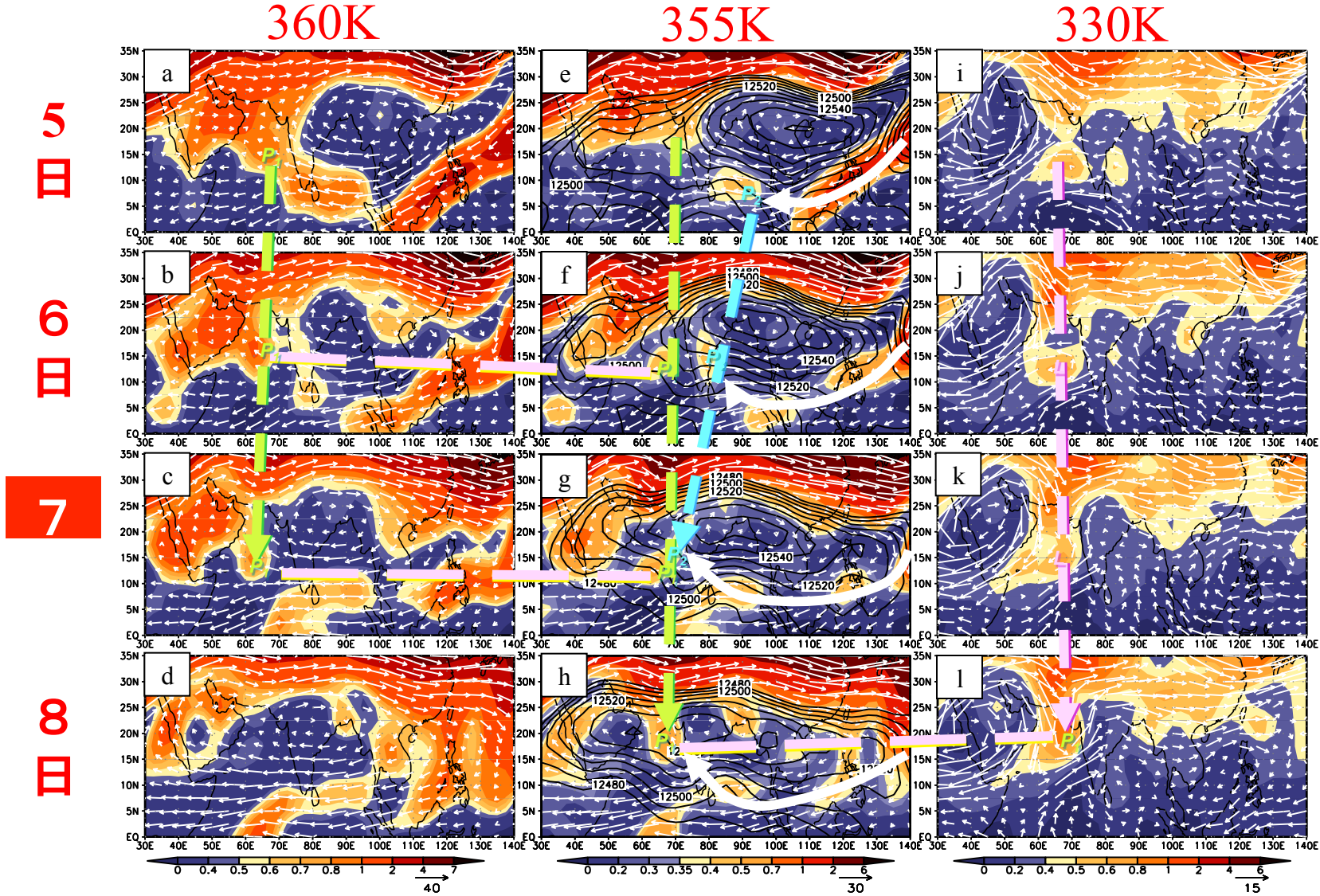


图8 6月在360K(a-d)、355K(e-h)、和 330 K (i-l) 等熵面上PV场(阴影, 单位: PVU)、风场(单位:m/s)和200hPa高度场(实线, 单位:gpm)的水平分布。第1-4行依序分别为5-8日。垂直虚箭矢表示对流层高层涡旋系统 P_1 , P_2 和对流层中层热带低压系统L的水平移动方向;水平粉红色长虚线指示低涡系统垂直向的锁相斜压发展。

Without friction: $k=0$, but N-S pressure gradient not uniform

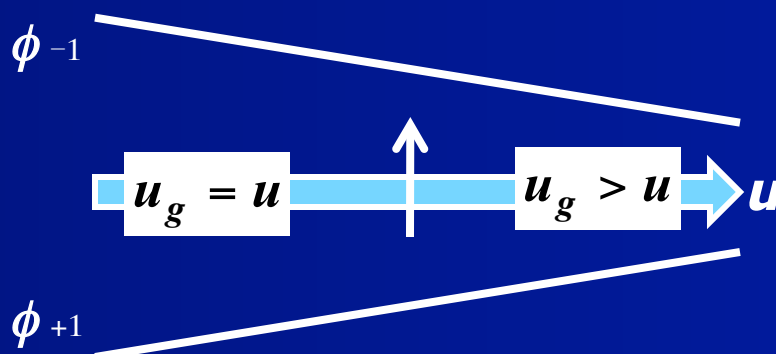
$$\frac{\partial}{\partial x} \left(\frac{\partial \phi}{\partial y} \right) \neq 0$$

$$\frac{D^2 v}{Dt^2} + \lambda^2 v = f(u \frac{\partial u_g}{\partial x}) \quad \lambda^2 = f(f - \frac{\partial u_g}{\partial y})$$

$$v_1 = \frac{1}{f - \frac{\partial u_g}{\partial y}} \left(\frac{\partial u_g}{\partial t} + u \frac{\partial u_g}{\partial x} \right) \approx \frac{1}{f - \frac{\partial u_g}{\partial y}} \cdot u \frac{\partial u_g}{\partial x} = -\lambda^{-2} u \frac{\partial}{\partial x} \left(\frac{\partial \phi}{\partial y} \right)$$

Mechanism

$$\frac{Dv}{Dt} = -fu + fu_g - Kv = f(u_g - u)$$



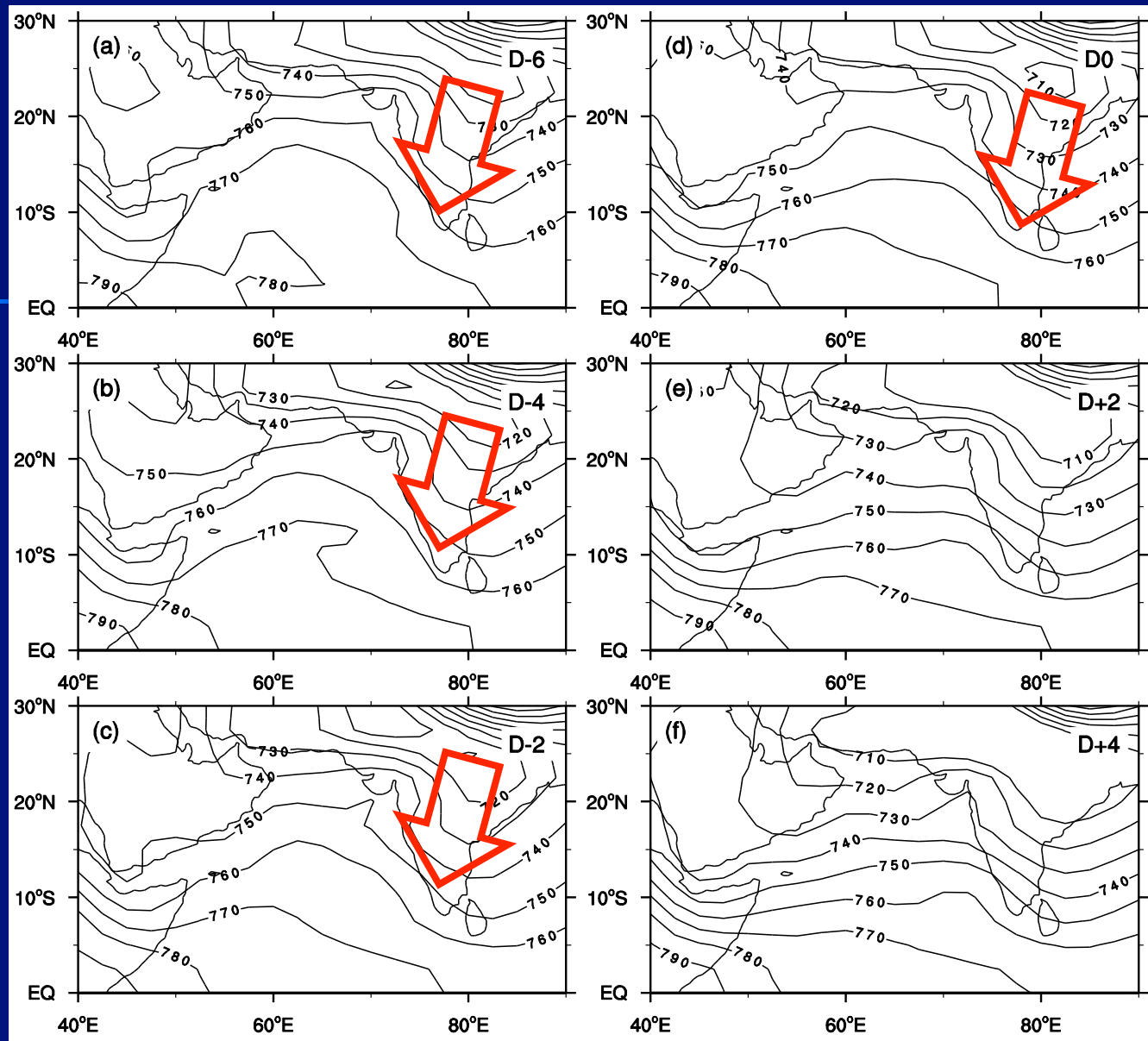
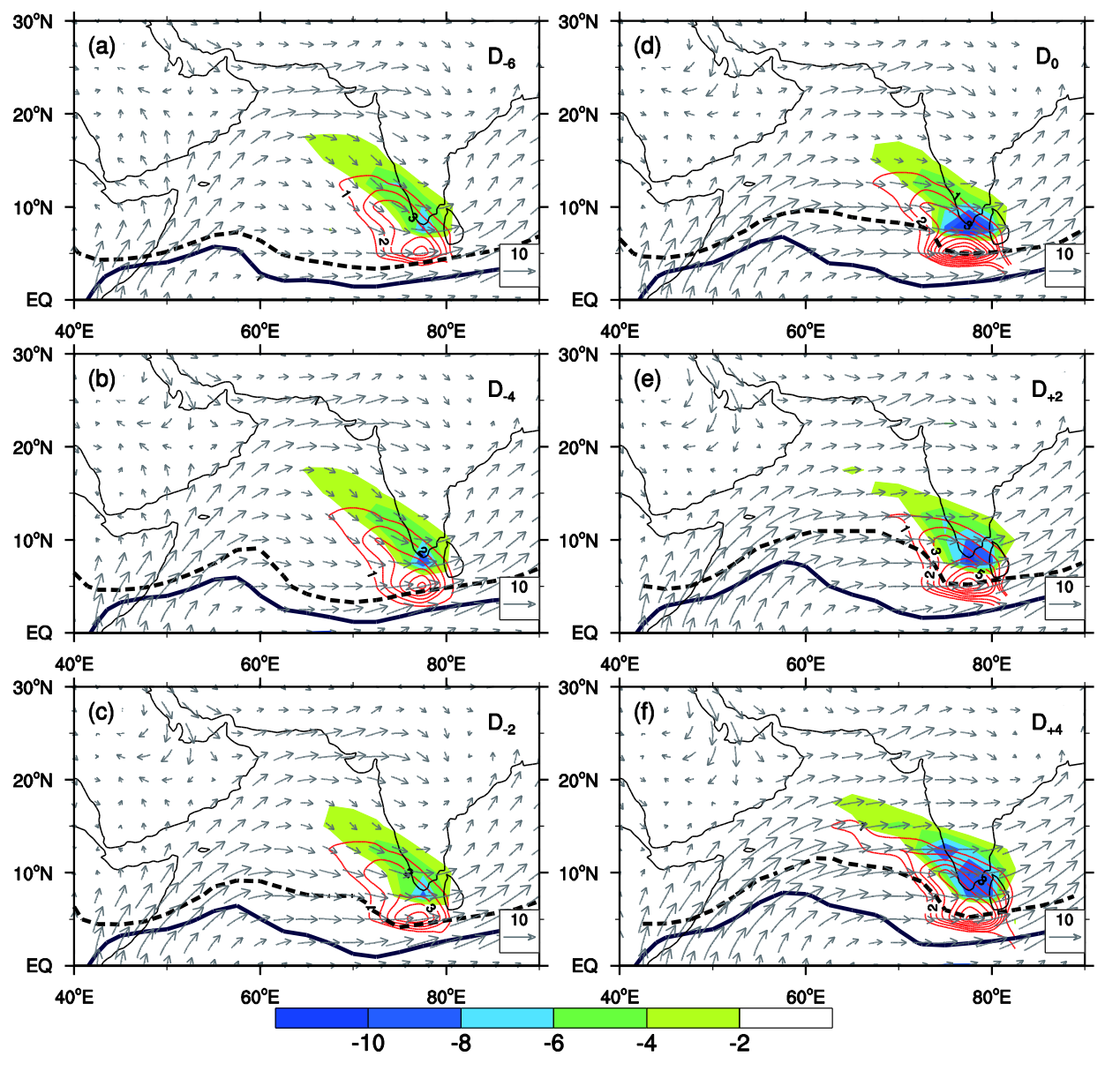
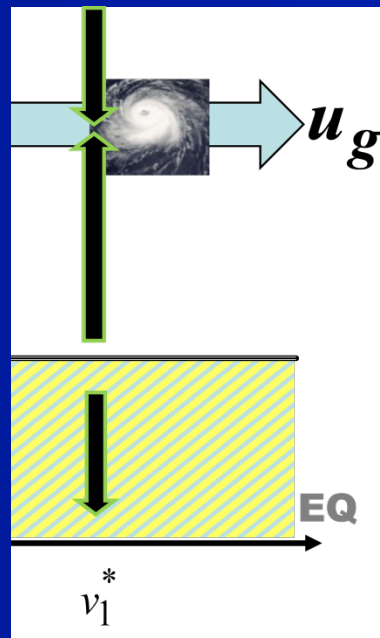


图 5 印度夏季风爆发过程中 925 hPa 等压面上位势高度(单位: dgpm)的演变特征。

Evolution of geopotential height at 925 hPa during the ISM onset (interval is 10 gpm)



$$v_1^* \approx -\lambda^2 \cdot u \frac{\partial}{\partial x} \left(\frac{\partial \varphi}{\partial y} \right)$$



强迫作用

图6 矢量: 925hPa风场 (m/s); ; 等值线: 925hPa v_1^* (m/s); 阴影:
 $d(v_1^*)/dy (10^{-6} s^{-1})$; 粗实线: 绝对涡度零线; 粗虚线: 地转西风急流轴

Previous review II: Onset process of Indian summer monsoon

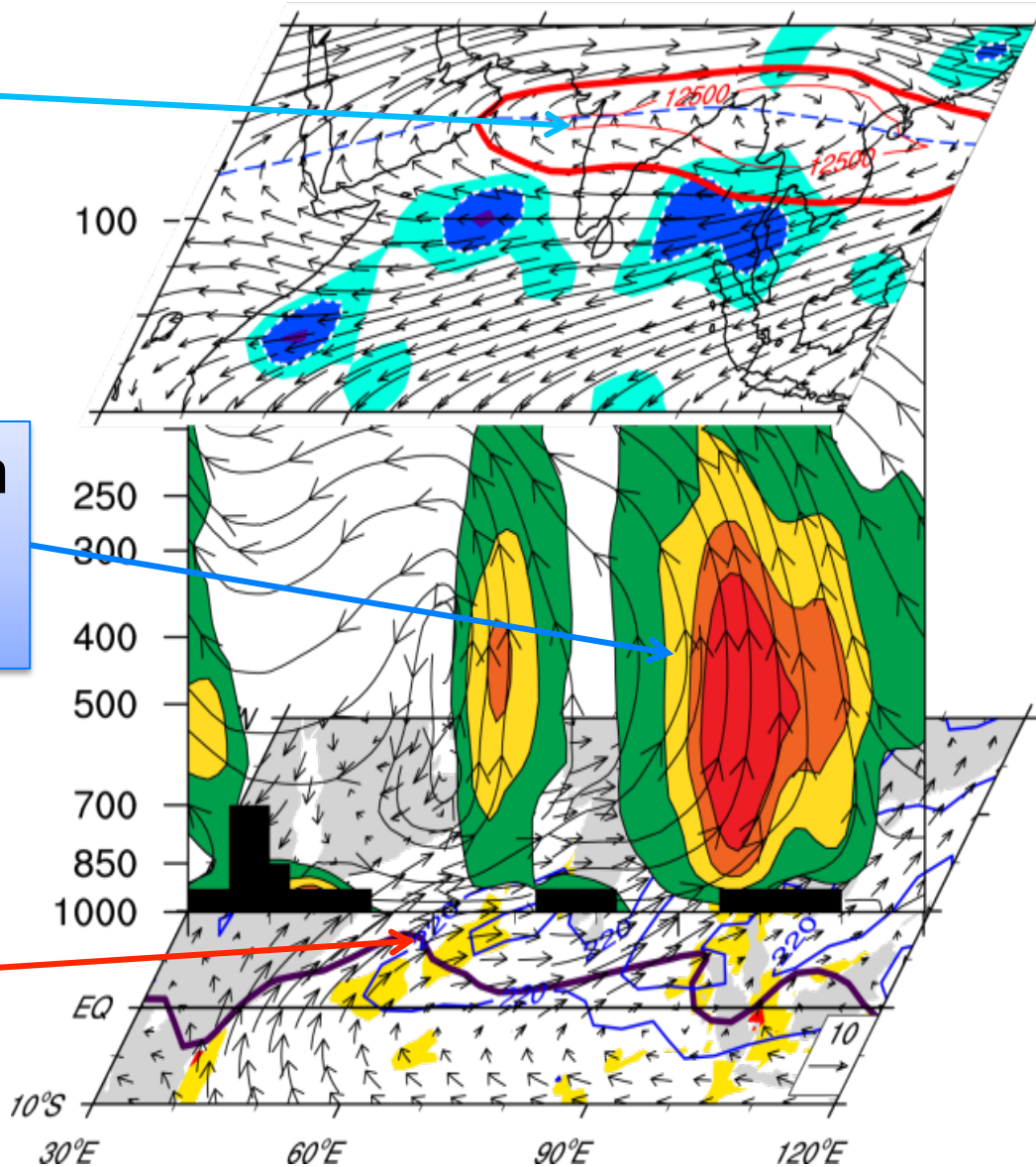
Upper-level: westward extension of SAH and its pattern variation (background)

Indian summer monsoon onset

BOB monsoon convection

$$v_1^* \approx -\frac{1}{\lambda^2} \left(u \frac{\partial}{\partial x} \right) \left(\frac{\partial \phi}{\partial y} \right)$$

Lower-level: Inertial instability and forced convection (trigger)



Outline

1

Introduction 引言

2

Dynamics of ASM onset

亚洲夏季风爆发动力学

3

Evolution of the ASM onset

亚洲夏季风爆发过程

4

ENSO and ASM Onset

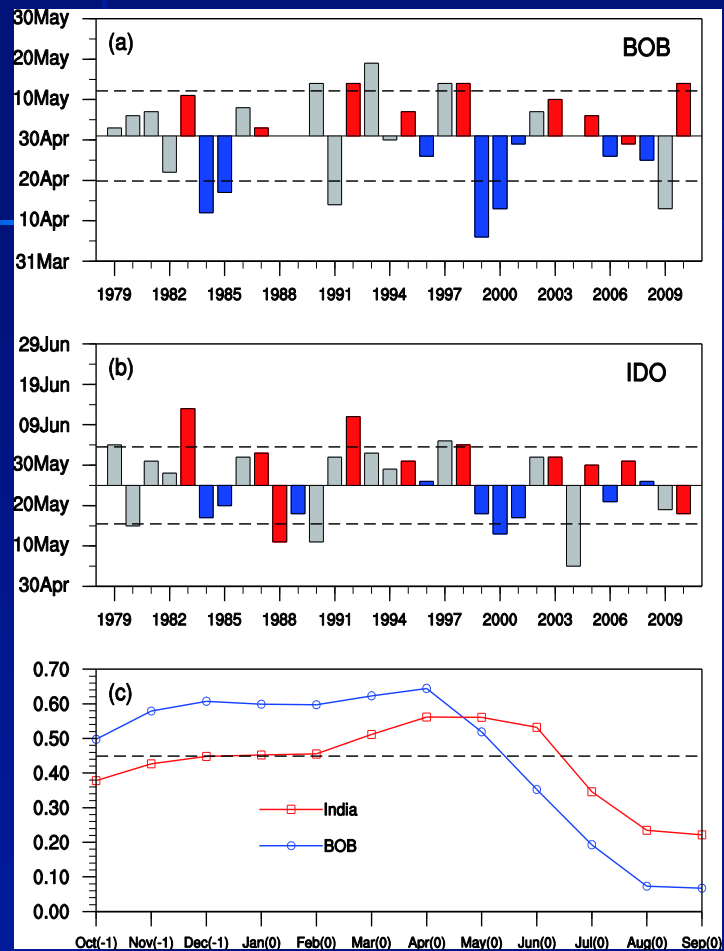
ENSO和亚洲夏季风爆发

5

Summary 结论



ENSO: one of the major factors influencing the interannual variability of SASM onset date



Onset dates of (a) BOB and (b) Indian summer monsoon; (c) lead-lag correlation of Niño3.4 SST with onset dates of BOB and Indian summer monsoon, respectively

- ◆ Red bars: warm ENSO occurred previously
- ◆ Blue bars: cold ENSO occurred previously

Possible impact processes of ENSO on ASM:

1. Anomalous Walker circulation and Atmospheric bridge;
2. Philippian sea anticyclone anomaly;
3. SAH formation and variation;
4. Land surface situation in previous winter and spring.

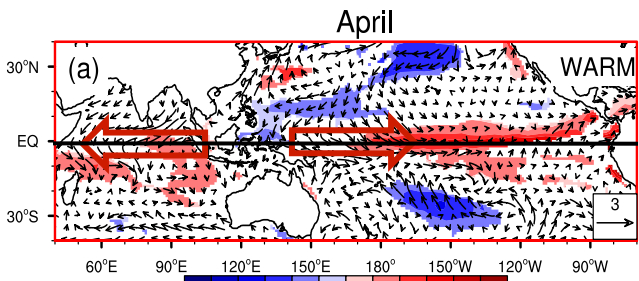
Scientific questions

- How does ENSO influence the interannual variability of ASM onset dates via the vertical coupling between upper- and lower-level circulation?
- Is the ENSO-impact process distinct among the different phase of ASM onset?

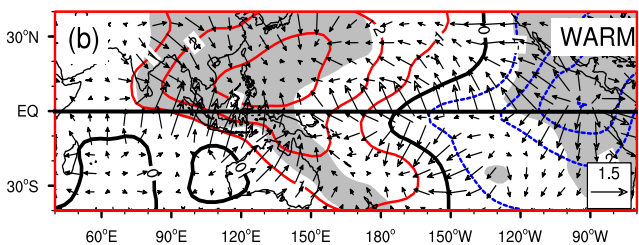
Composite analysis: Anomalous large-scale atmospheric circulation in different phases of ENSO



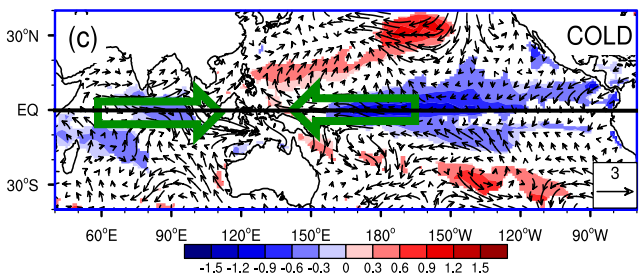
Warm ENSO
SSTA(K)&sea surface wind($m s^{-1}$)



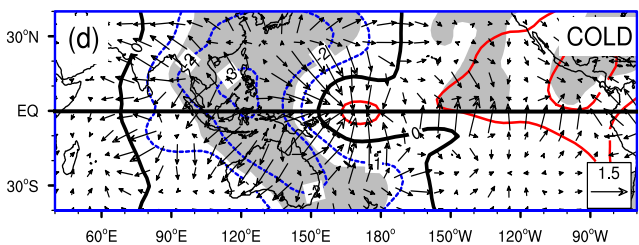
Warm ENSO
200-hPa velocity potential ($10^{-6} s^{-1}$)& divergent wind ($m s^{-1}$)



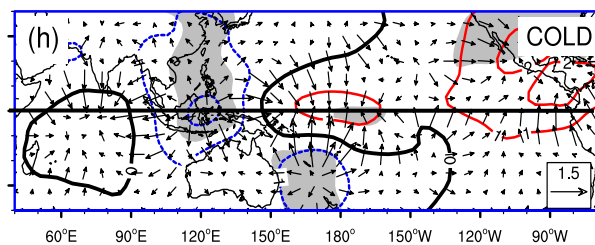
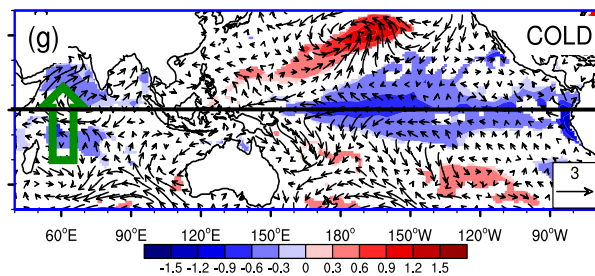
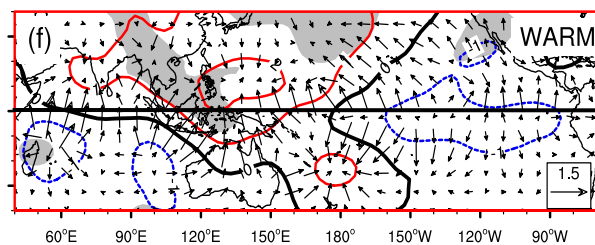
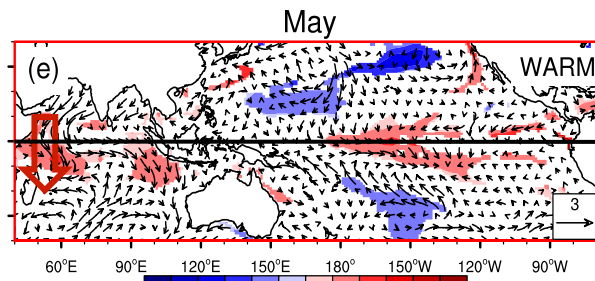
Cold ENSO
SSTA(K)& Sea surface wind($m s^{-1}$)



Cold ENSO
200-hPa velocity potential ($10^{-6} s^{-1}$)& divergent wind($m s^{-1}$)



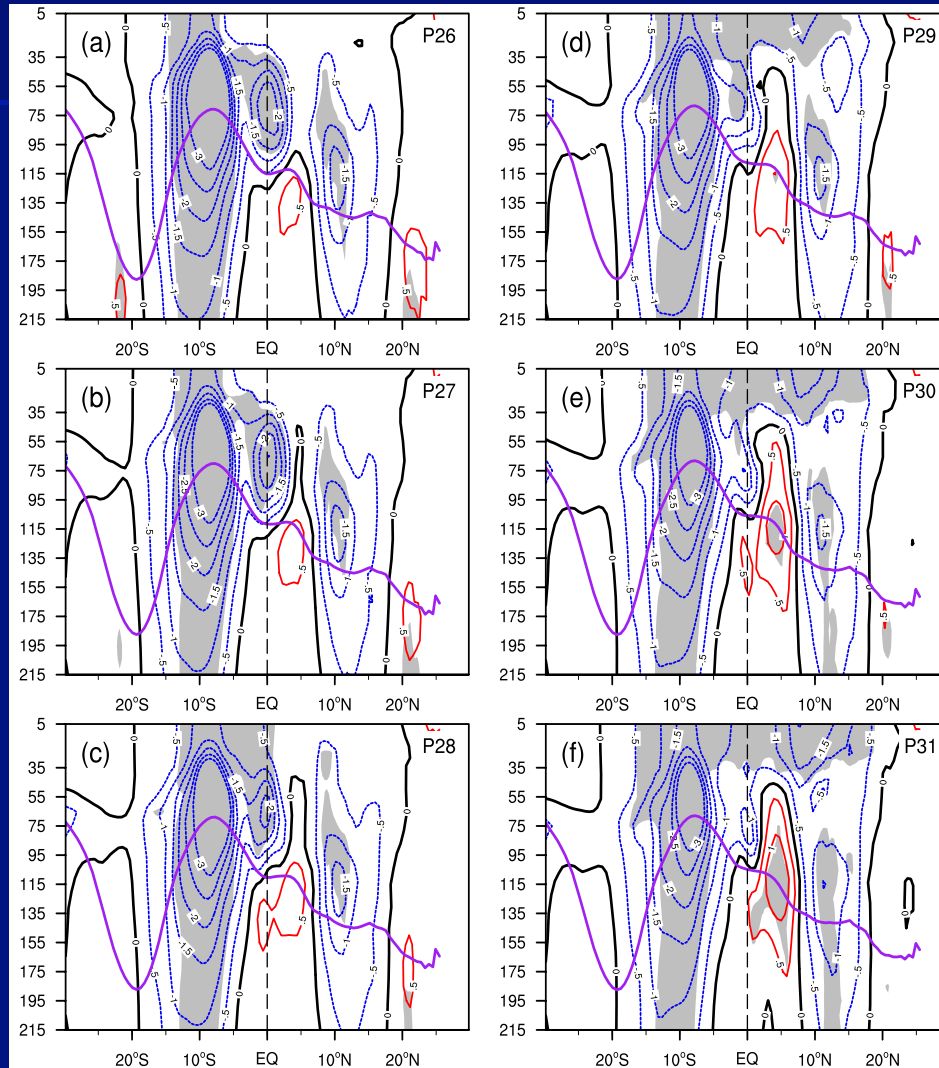
April: Zonal SSTA gradient
in tropical Indo-Pacific Ocean



May: Meridional SSTA gradient
in Arabian Sea

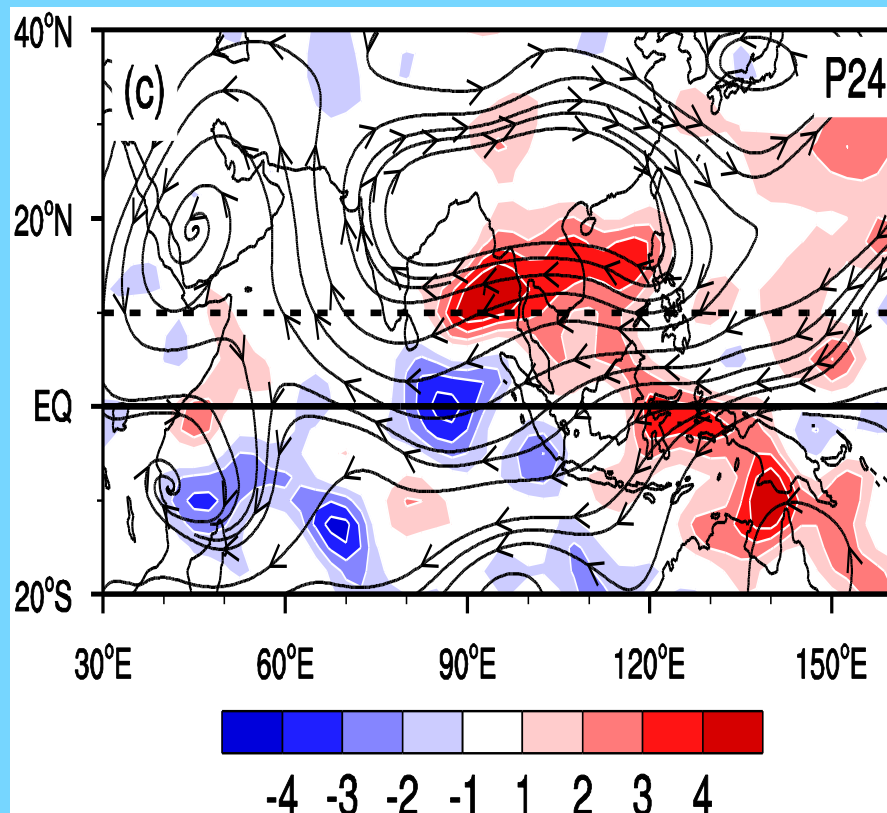
Reason for the Indian Ocean SSTA in May: local meridional asymmetric distribution of thermocline

50°-70°E averaged depth-latitudinal crossing section of subsurface temperature anomalies (K); Purple lines: climate-mean position of thermocline (D20)

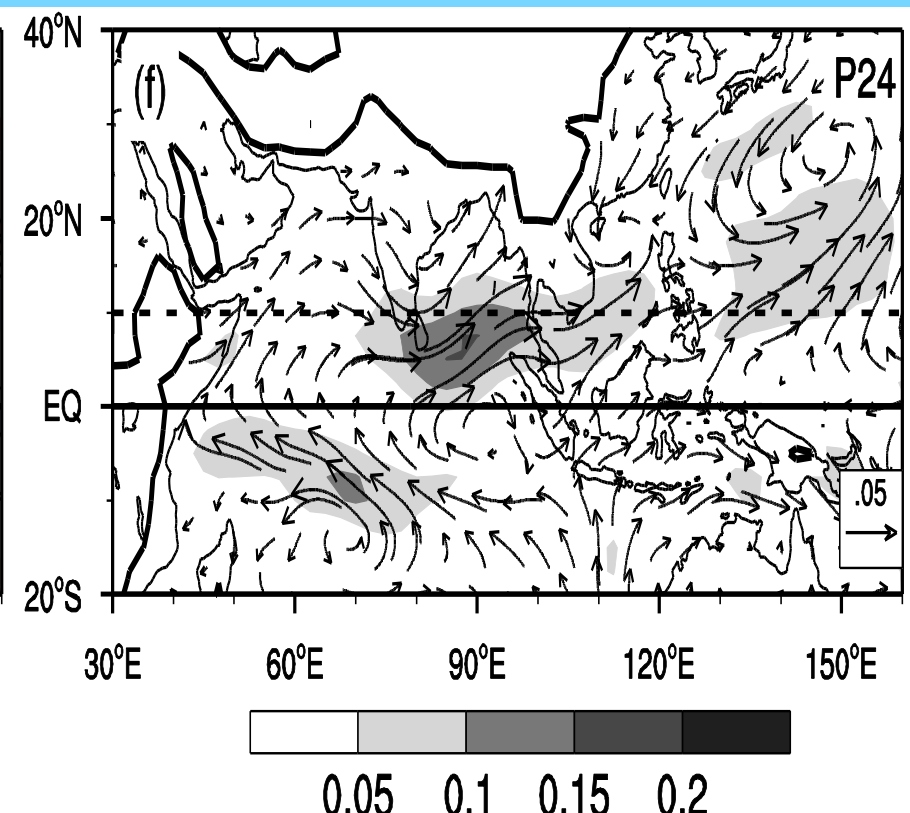


April: ENSO influences on the upper- and lower-level circulation during the BOB summer monsoon onset

200-hPa Streamline & 500-hPa Q_1



925-hPa moisture transport

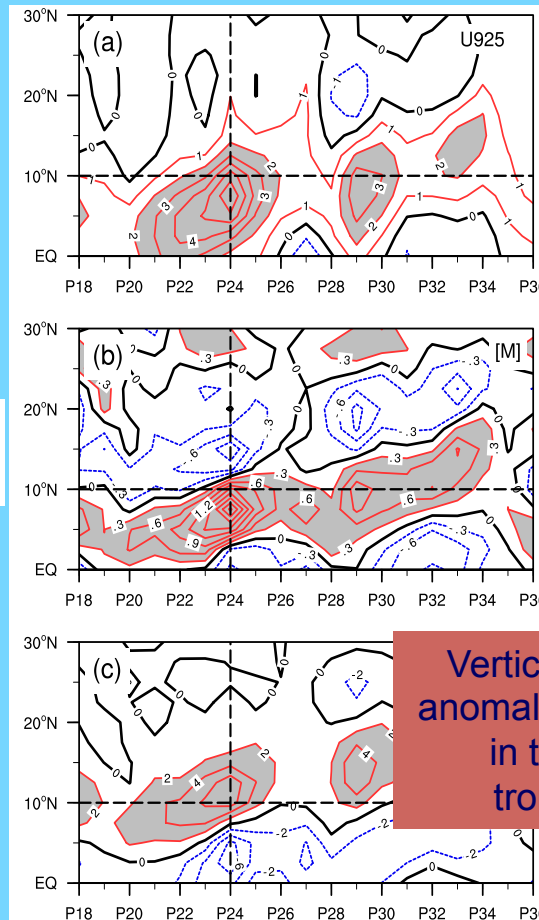


Cold ENSO-Warm ENSO

April: ENSO influences on the upper- and lower-level circulation during the BOB summer monsoon onset

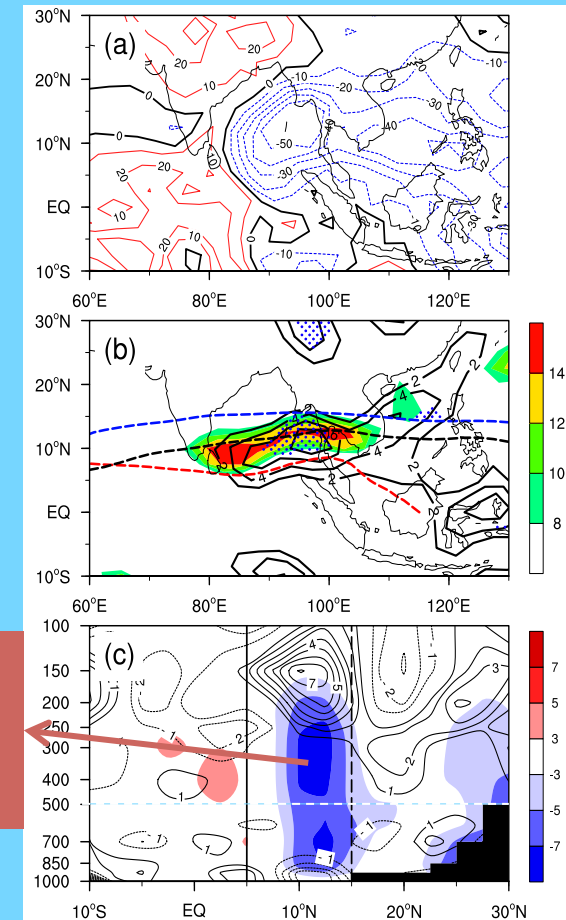
Lower-level: Barotropical instability is strengthened over southern BOB following cold ENSO

Zonal wind anomalies

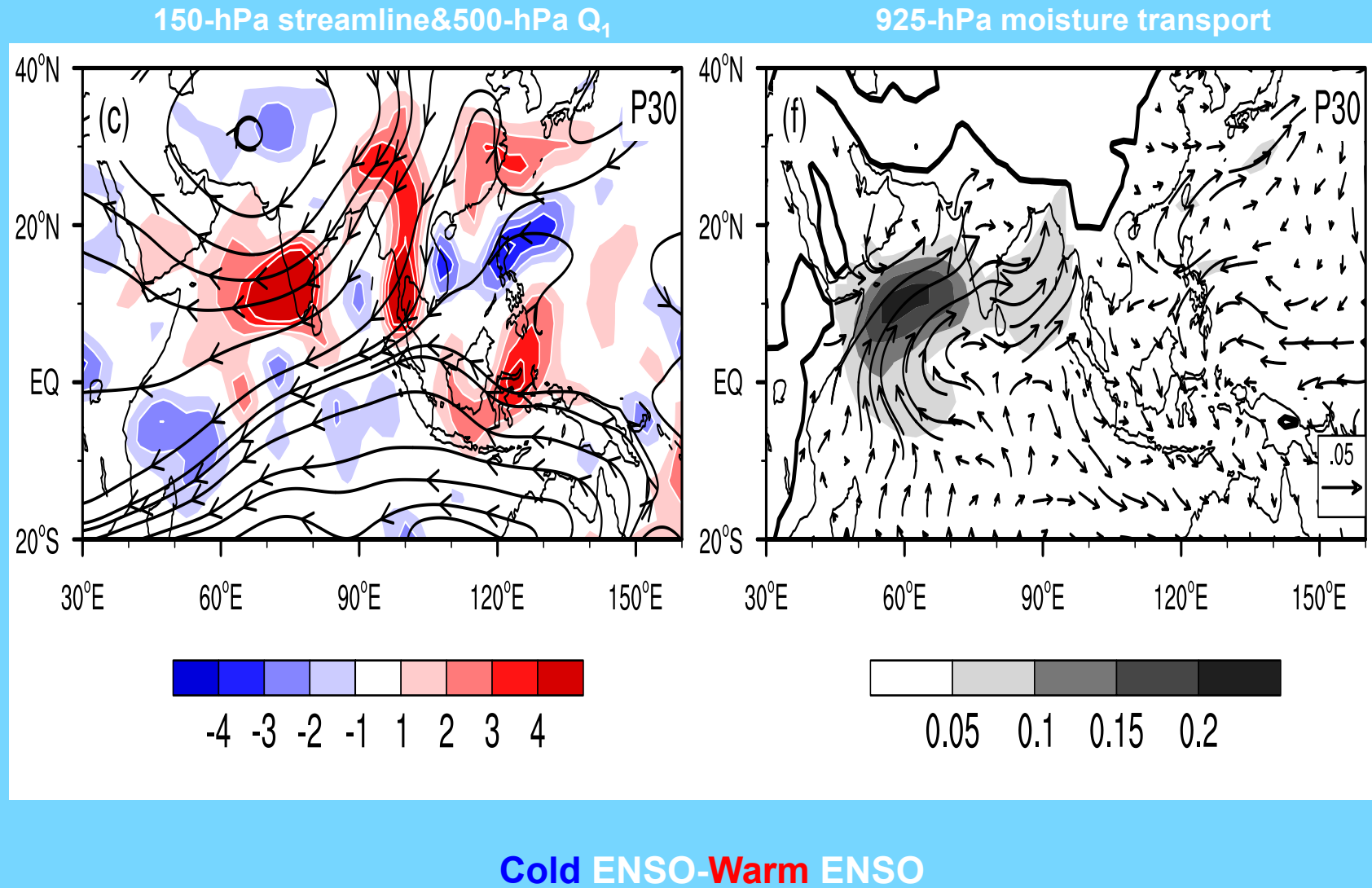


Upper-level: SAH is to the north of its climate-mean position, enhancing the divergence-pumping over northern BOB

OLR

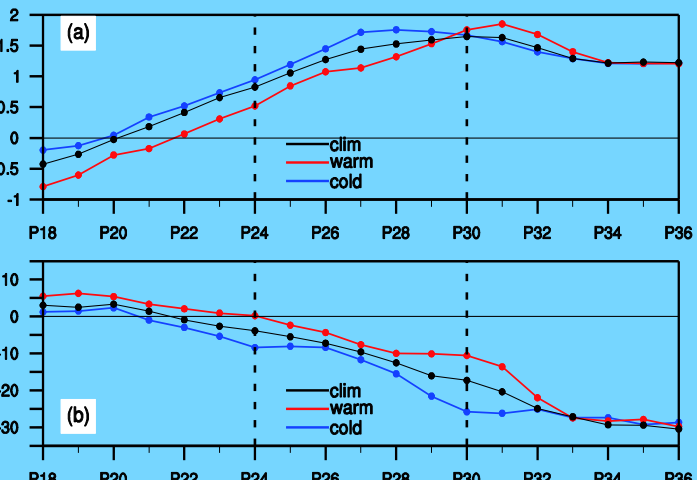


May: ENSO influences on the upper- and lower- level circulation during the Indian summer monsoon onset

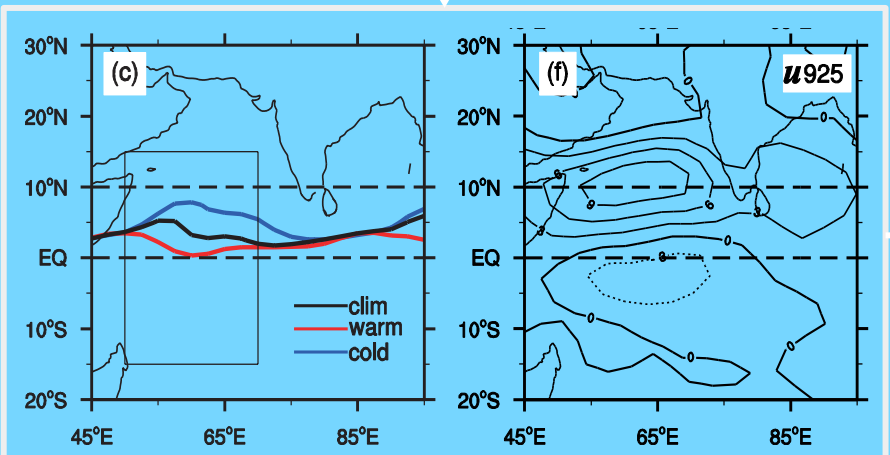


May: ENSO impact on the lower-level inertial instability and forced convection over Arabian Sea during Indian summer monsoon onset

Cross-equatorial SSTA gradient in Arabian Sea->
Meridional gradient of anomalous SLP

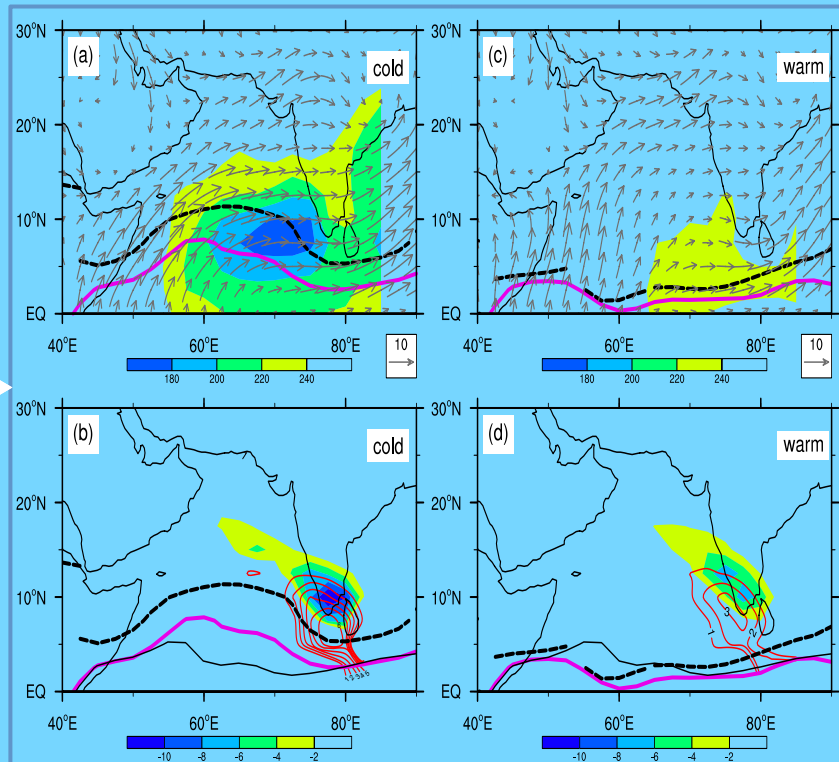


Inertial instability



Cold ENSO-Warm ENSO

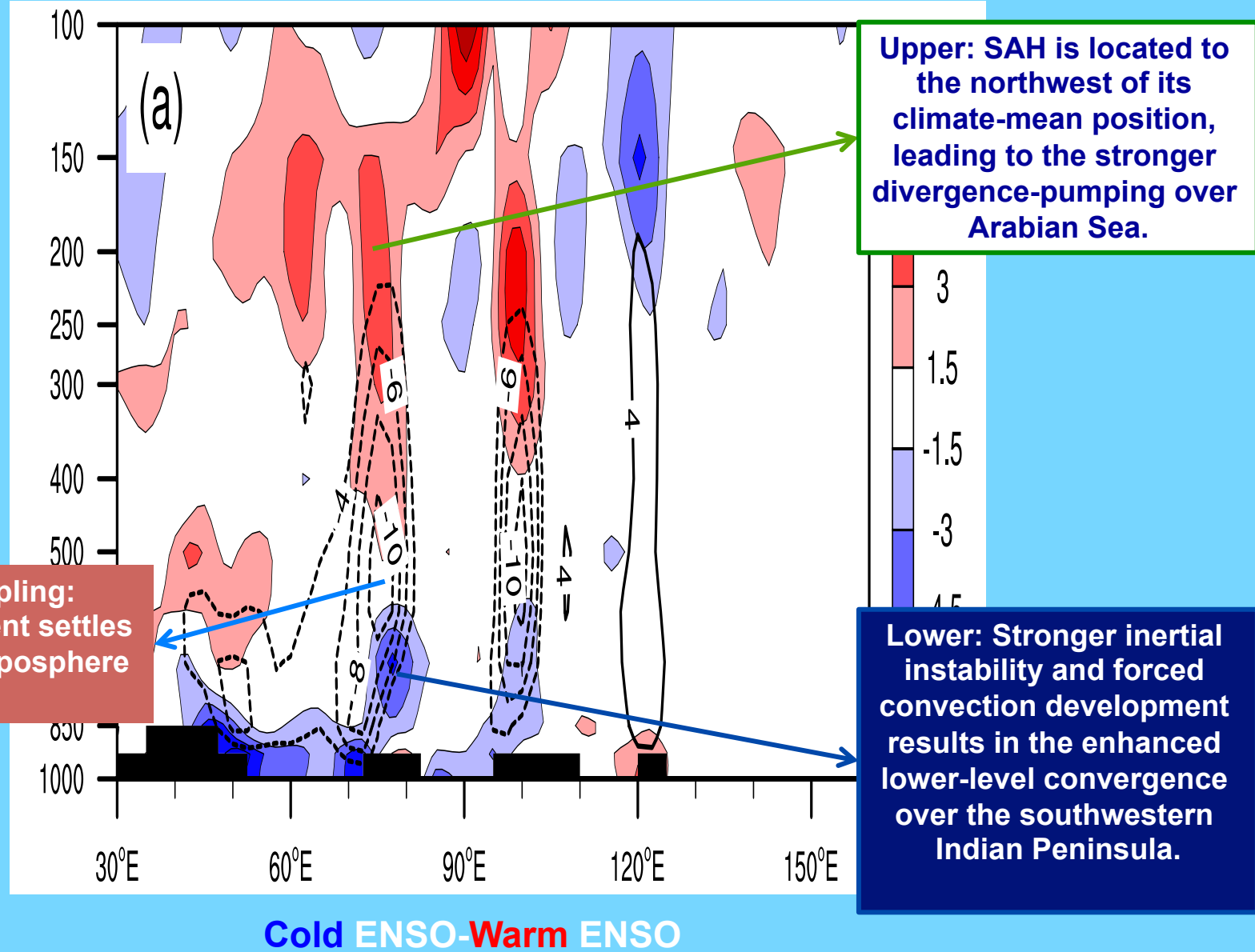
Forced convection development



$$v_1^* \approx -\frac{1}{\lambda^2} \left(u \frac{\partial}{\partial x} \right) \left(\frac{\partial \phi}{\partial y} \right)$$

May: ENSO effect on the vertical coupling between upper- and lower-level atmospheric circulation of Indian summer monsoon onset

Divergence
(shading) &
omega (contour)



Outline

1

Introduction 引言

2

Dynamics of ASM onset

亚洲夏季风爆发动力学

3

Evolution of the ASM onset

亚洲夏季风爆发过程

4

ENSO and ASM Onset

ENSO和亚洲夏季风爆发

5

Summary 结论



Summary and discussion

1. ENSO can alter the onset dates of SASM via changing the vertical coupling between upper- and lower-level circulation over SASM region.
2. In the interannual timescale, the SAH response to ENSO in the upper troposphere is important for the anomalous SASM onset.
3. The change in the near equatorial E-W SSTA gradient in the Indo-Pacific Ocean is responsible for the anomalous BOB summer monsoon onset.
4. The change in the cross-equatorial (N-S) SSTA gradient in the western Arabian Sea can result in the changes of inertial instability and forced convection development in the lower troposphere , causing anomalous Indian summer monsoon onset.

结论和讨论

1. 通过改变热带印度 - 太平洋的海表温度梯度，ENSO显著的影响着亚洲季风区大气环流高低空的耦合，从而影响着亚洲季风的爆发；
2. 冷/暖ENSO年高层南亚高压发展早/迟，对亚洲夏季风爆发的年际变化有重要的影响；
3. 冷/暖ENSO年印度洋 - 太平洋近赤道异常的东西向SST梯度是导致孟加拉湾夏季风提前/推迟爆发的原因；
4. 冷/暖ENSO年西阿拉伯海跨赤道异常的南北向SST梯度是导致异常的惯性不稳定和强迫对流发展，从而引起印度夏季风提前/推迟爆发的原因。

Thank You!

